ISTITUTO NAZIONALE DI FISICA NUCLEARE

Sezione di Torino

INFN/AE-03/03
12 Giugno 2003

ULTRA
UV LIGHT TRANSMISSION AND REFLECTION IN THE ATMOSPHERE TECHNICAL REPORT

A SUPPORTING EXPERIMENT FOR THE EUSO PROJECT

Osvaldo Catalano[1], Piero Vallania[2], Didier Lebrun[3], Patrick Stassi[3], Mario Pimenta[4], Catarina Espirito Santo[4]

[1)]INFN-Sezione di Catania and CNR-IASF Sezione di Palermo,Italy
[2)]INFN-Sezione di Torino and CNR-IFSI Sezione di Torino, Italy
[3)]ISN Grenoble, France
[4)]LIP Lisboa, Portugal

Abstract

The ULTRA experiment has been designed in the framework of the EUSO project to provide quantitative measurements of the reflected/diffused signal produced by the EAS impacting on the Earth surface. The detector is a hybrid system consisting of an UV optical detection unit, the UVscope, and an array of scintillators, the ETscope (EAS Telescope). The UVscope is used to detect Cherenkov diffused UV light from EAS which are detected in coincidence by the ETscope array. The atmospheric transmission properties will also be studied using the UV light detector and a laser emitter. Moreover, measurements of light from meteors are feasible with the same instrumentation.

In this paper the various physical items involved in this research are introduced and discussed, and a detailed project of the experimental setup together with preliminary estimations of the expected performances are presented.

PACS 98.70.Sa – Cosmic rays.
PACS 96.40.Pq – Extensive air showers.
PACS 95.55.Vj – Neutrino, muon, pion and other elementary particle detectors; cosmic ray detectors.
PACS 07.87.+v – Space borne and space research instruments, apparatus and components.

Published by ***SIS–Pubblicazioni***
Laboratori Nazionali di Frascati

1. INTRODUCTION

The EUSO-Extreme Universe Space Observatory experiment[1)] has been proposed to the European Space Agency (ESA) on January 2000 in response to the Announcement of Opportunity for F2/F3 missions. EUSO was selected by ESA for an accomodation study on the International Space Station (ISS)[2)]. On March 2002 a one year phase A study was initiated, during which the EUSO Payload and Instrument must be assessed in all the relevant parts. Conventionally the Payload defines the ground segment and the Integrated Flight segment including Instrument, robotics, transportation and installation on the ISS (comprising all the necessary items and activities on the ISS). The Instrument identifies the physical unit of the Payload that contains all the scientific equipment, support equipment and structural elements of the EUSO mission as external experiment of the ISS. The Instrument design is on charge of the EUSO scientific consortium while the Payload is on charge of the ESA Science and Manned Space Flight and Microgravity directorates.

The primary purpose of EUSO is to detect, with high event statistics, Extreme Energy Cosmic Rays (EECR) and neutrinos, that may be indicative of unknown production and acceleration mechanisms in the Universe. EUSO will look downwards to the Earth atmosphere, from an altitude of about 400 km, and image the fluorescence ultraviolet (UV) faint traces produced by the charged secondary particles in the Extensive Air Showers (EAS) initiated by relativistic primary particles, along their development in the Earth atmosphere. The Cherenkov light accompanying the shower and reflected/diffused back by the Earth surface will also be detected. Other objectives include measurements of meteor light curves, blue jets, sprites and other atmospheric phenomena, by detecting the associated fluorescence light.
The EUSO Instrument uses a large Fresnel wide-angle optics (field of view FOV=60°) concentrating the UV photons on a large focal surface made of thousands of multipixel phototubes. The detected UV photons, coming out from the superposition of the event signal, correlated in space and time, to the uncorrelated background, are digitized in predefined Gate Time Units (GTU) of the order of a microsecond. System electronics governing the instrument takes care of the overall triggering and data taking operations up to the data selection for transmission.

Laboratory and ground based experiments have been identified, in the context of EUSO, as propaedeutic experimental supporting activities.
Since 1998, atmospheric background measurements have been performed by balloon borne experiments in the wavelength interval relevant for EUSO. Over ground and over sea background radiance profiles have been obtained using data from the BABY[3)] and BABY2002 balloon flights. Other flights are foreseen in the future from different latitudes and under different environmental conditions.
Background measurements at mountain altitude, looking at the nocturnal sky, have also been performed in the last year, providing information on several parameters as diffuse background intensity at different moon phases and inclinations. Observations from ground of stars with known light spectrum have been used as source-candles to calibrate the detectors, similar to those used in the BABY experiment. Using the same apparatus, an observation program for meteoroids detection from ground in the 300-400 nm wavelength band has already started and signatures from meteoroids in the instrument field of view are expected during the sporadic meteor showers.

Laboratory measurements of fluorescence yield at low energy (22 KeV)[4], using the X-ray facilities located in Palermo, have been performed in 1999, whereas the possibility of measurements at higher energies, of basic importance for the project, is presently under discussion within the EUSO collaboration.
The transmission characteristics in the atmosphere and the reflection/diffusion over land and clouds of the light associated to extensive air showers, which are another crucial subject for EUSO, are covered in this proposal.

The ULTRA (Uv Light Transmission and Reflection in the Atmosphere) experiment has been designed to provide quantitative measurements of the reflection/diffusion signal produced by the EAS impacting on the Earth surface, overcoming the lack of information in this specific field. A scintillator array (using conventional sampling technique) and UV light detectors (300-400 nm wavelength interval) will operate simultaneously to detect EAS in coincidence with the UV light reflected/diffused from its impact on Earth. The atmospheric transmission properties will also be studied using the UV light detectors and a laser emitter. Moreover, measurements of light from meteors are feasible with the same instrumentation.

This document is organized as follows. Section 2 illustrates in a very essential and concise way the main aspects that constitute the framework for the proposed measurements. They are introduced as starting points, gathering basic information. To deal with these topics exhaustively more calculations and Monte Carlo simulations will have to be developed. In section 3 the topic of meteor observation within the ULTRA program is introduced and discussed. In section 4 the physical objectives are discussed and the apparatus is described. The experiment geometry and design parameters are discussed in further detail in section 5.

2. UV LIGHT FROM EAS IN THE ATMOSPHERE

2.1 EAS development in the atmosphere

The interaction of a primary cosmic ray of energy E with the atmospheric nuclei (mainly Nitrogen) produces a shower of particles. The conventional form used for the total number of electrons in a photon-initiated shower is (Greisen[5]):

$$N(t) \sim 0.31 \exp[t(1-3/2 \ln s)]/(ß_0)^{½} \quad (2.1)$$

where:

$$t = p(g/cm^2)/ (r.l. = 37.1\ g/cm^2) \quad (2.2)$$

$$ß_0 = \ln [E/(E_c = 81\ MeV)] \quad (2.3)$$

$$s = 3t/(t + 2\ ß_0\ ) \quad (2.4)$$

The shower development is thus mainly driven by two parameters: the radiation length (r.l.) and the critical energy (E_c). A combination of these parameters gives the shower age s (s=1 at the shower maximum).

At the detection level the shower size has a lateral distribution that is usually referred as the NKG formula[5,6]:

$$\rho(r) = c(s)\ N_e/r_0^2\ (r/r_0)^{s-2}\ (1+r/r_0)^{s-4.5} \quad (2.5)$$

where r_0 is the Molière radius (~ 100 m) and:

$$c(s) = 0.366\ s^2\ (2.07 - s)^{1.25} \tag{2.6}$$

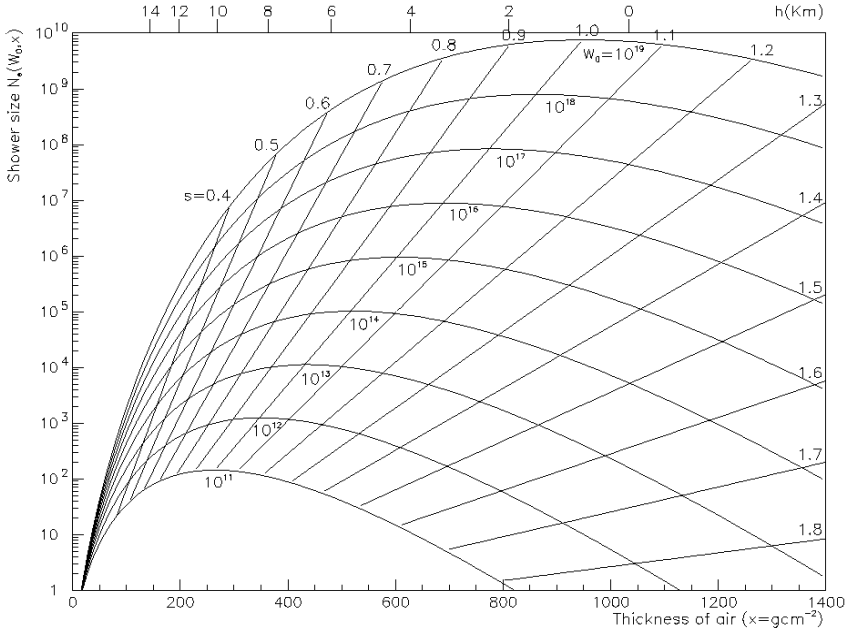

Fig. 1: Longitudinal development of EAS in air for energies ranging from 10^{11} to 10^{19} eV, as parameterized by the Greisen formula (2.1).

For showers initiated by hadrons only part of the energy (~ 50%) goes into the electromagnetic component. A possible parameterisation of the longitudinal profile of a hadron-initiated EAS has been proposed, as a modification of Greisen formula, by John Linsley (John Linsley, private communication) and is discussed, for instance, in Ref.[7)]
The EAS detection is done with different techniques, focusing in the different components of the EAS (electrons, muons, photons and hadrons); the detector array technique measures mainly the electromagnetic component of EAS, sampling the lateral distribution of the showers with unshielded thin detectors scattered on the ground.
With this technique it is not possible to distinguish the different shower components, but the electrons are much more numerous than hadrons or muons.

From figure 1 it is clear that the shower maximum is reached above the sea level, at least for photons up to E = 10^{19}eV (vertical showers; the energy is even larger for inclined showers, since the slant depth to reach the maximum remains unchanged and is reached at higher altitude). For this reason it is convenient to detect the EAS at mountain altitudes, where the total number of particles is larger. Figure 2 shows the lateral distribution for EAS with shower size $N_e > 10^5$, measured at 2000 m a.s.l.[8)] and fitted with equation (2.5). The conversion from shower size to energy/nucleus depends on the detection level and is a critical issue for three main reasons:

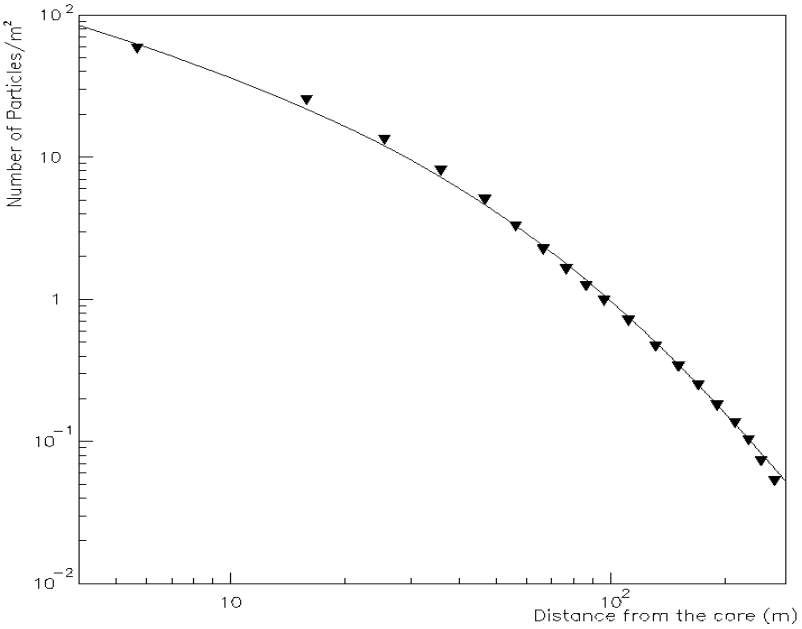

Fig. 2: Mean experimental lateral distribution of EAS, measured at 2000 m a.s.l., for showers with $N_e > 10^5$ [8]. The line is the best fit to the NKG formula (2.5).

1) N_e fluctuations at the same primary energy are ~ 100%, mainly due to the fluctuations of the first interaction point;
2) The conversion depends on the primary mass, with a factor of ~ 2 uncertainty for primaries ranging from proton to iron.
3) The conversion depends on the interaction model assumed, since no direct measurements are available for $E > 10^{14}$ eV (maximum energy $E_{lab} \approx 1.7 \cdot 10^{15}$ eV at Tevatron for p-pbar, while the direct information on nucleus-nucleus interaction, e.g. S-S, is limited to $6.4 \cdot 10^{12}$ eV at SpS. Moreover the available data in accelerator experiments are usually obtained in a rapidity range different from the region relevant to cosmic-ray data.

2.2 Fluorescence light production

EUSO will detect the EECR by looking at the streak of fluorescent light produced when the EAS particles interact with the atmosphere of Earth. Electrons moving through the atmosphere ionize the air and excite metastable energy levels in its atoms and molecules. With a short relaxation time, they come back to the ground state emitting a characteristic fluorescent light. In air, fluorescence extends from infrared to UV, with peaks at wavelengths from 330 to 450 nm. The UV yield is of the order of 4 photons per meter per charged particle. The emitted light is isotropic and proportional to the shower energy at any given depth in the atmosphere. Observation of this light at distance from the shower axis is the best way to control the cascade longitudinal profile of the EAS.

The basic information returned by the EUSO detector will be an ensemble of shower curves giving the ionization as a function of slant depth X in the atmosphere for each shower, together with its trajectory. An important feature of EUSO with respect to ground based fluorescence detectors, is the negligible contribution of the “proximity” effect (showers are

nearly equidistant from the detector, since the radiating part of the atmosphere is seen as a thin sheet (~30 Km thick) from a far eye (~400 Km is the mean value for the ISS orbit)). This characteristic enhances the capability for direct unbiased visual recording of the shower longitudinal development. The possibility of knowing about the depth at the maximum of the shower development, X_{max}, makes it possible study the primary chemical composition shower by shower. Moreover, the knowledge of the absolute X_{max} value is of fundamental importance to separate hadronic showers from neutrinos showers.

2.3 Cherenkov light production

The electrons in the EAS generate not only fluorescence light but also a rather prodigious amount of Cherenkov light, which is highly beamed in the forward direction. The Cherenkov light builds up with the shower front and it lands on the Earth surface or in the clouds, where it is partially absorbed and partially reflectively diffused. EUSO will take

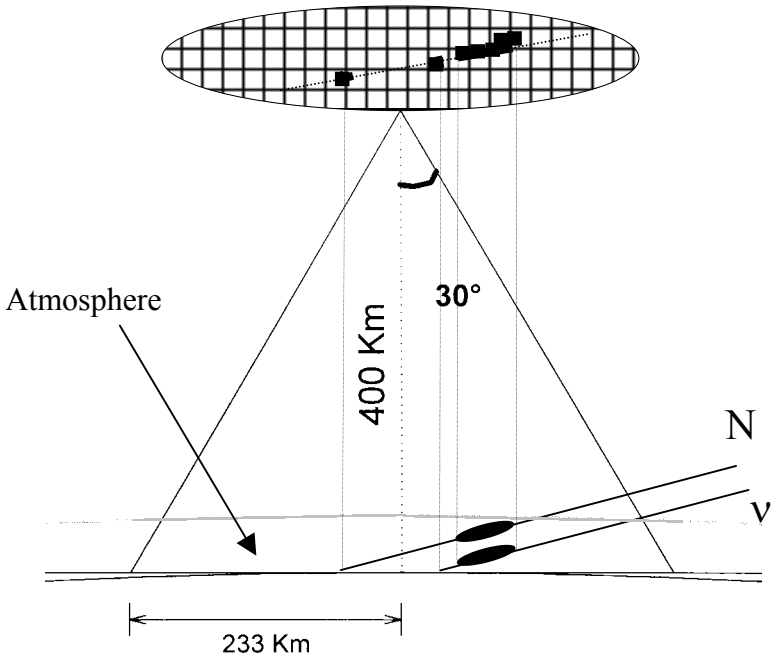

Fig. 3: Neutrino shower and hadron shower as imaged by the EUSO focal surface detector. Note as the Cherenkov signature permits to resolve high penetrating neutrino from quick interacting hadron.

advantage of the diffused Cherenkov photons using them as signature of the impact point of the shower front in the surface. This signal, together with auxiliary altimeter information, will permit to measure X_{max} with a precision of few tens of g/cm^2. For the sake of clarity a sketch of the reported geometry is shown in figure 3. Moreover, Cherenkov light could be used as an independent estimation of the energy of the shower if the reflectivity of the shower landing surface is known. EAS detection via Cherenkov light reflection from snowed surface was first proposed by A.E. Chudakov in 1972[9] and performed at the Big Alma-Ata Lake (Kazakhstan)

and other sites since 1983[10,11,12]; the obtained differential energy spectrum of cosmic rays in the range 10^{16}-10^{17} eV agrees well with measurements based on other techniques.

Cherenkov radiation is produced by cosmic ray particles traversing the atmosphere. As already stated, Cherenkov light builds up with the shower front and it is highly beamed in the forward direction. At sea level and for a relativistic electron (E>21 MeV) the maximum value for the Cherenkov angle is $\vartheta_{max} = 1.3°$. For this feature the Cherenkov light gives a small contribution to the detected signal from space, whilst it is strong enough to be detected when it bounces off a surface. Another feature of Cherenkov light consists in the short duration of the light flash. At ground observation level, the depth of the Cherenkov light is of the order of less than 10 ns. Its duration depends from the shower inclination and the optical property of the reflecting surface (ocean, desert, forest, clouds,...) and the light intensity, as a function of the distance **r** from the "core axis" of the shower may be represented, if dispersion is neglected, in the form:

$$I(r) \propto 1/r \cdot e^{-h/2\lambda} \qquad (2.7)$$

where **h** is the light generation height and $\lambda \approx$ **7.4** km is the characteristic scale height of the atmosphere.
Figure 4 shows the simple geometry involved in the determination of the maximum radius of

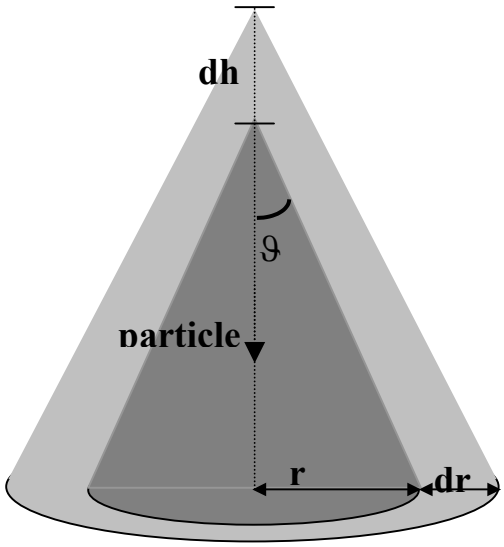

Fig. 4: Lateral distribution of Cherenkov light on ground produced by a single charged particle. The light intensity generated in a height interval **dh** and falling in an annulus of radius **r** in absence of Coulomb scattering.

the pool of light. For a single fast electron traversing the atmosphere vertically, neglecting scattering of the electron as well as scattering and refraction of the light, the Cherenkov light generated at an height **h** and at an angle ϑ arrives at the ground at a point distant **r** so that:

$$r = h \cdot \vartheta \; . \qquad (2.8)$$

The refraction index of air at sea level, **n,** is close to unit:

$$n=1+\rho_0 \tag{2.9}$$

where ρ_0 **=2.9** $\cdot$**10**$^{-4}$. Since the refractive index is proportional to the density and the density varies exponentially with atmosphere, a suitable parameterisation is:

$$\rho=\rho_0 \cdot e^{-h/\lambda} \tag{2.10}$$

Using the Cherenkov relation **cos** ϑ**=1/(**$\beta\cdot$**n)**, it can be shown that the maximum value of Cherenkov angle, for β**=1**, is:

$$\vartheta \approx \sqrt{2\cdot\rho} \tag{2.11}$$

From equation (2.11) and (2.8), the radius of the light cone at sea level is:

$$r = \sqrt{2\cdot\rho_0} \cdot h \cdot e^{-h/2\lambda} \tag{2.12}$$

It is straightforward, from equation (2.12), to calculate the $\mathbf{r_{max}}$, that is obtained for $\mathbf{h_{max}=2\lambda}$ and is found to be about 130 m.

2.4 Transmission in the atmosphere

In order to accurately interpret the optical signal associated to EAS, it is necessary to know by what factor light is attenuated when passing through the atmosphere. As absorption is negligible in the relevant wavelength interval (300-400 nm), the main contribution to the light attenuation is given by scattering from particles with size larger than the wavelength of light, referred to as Mie scattering[13], and by scattering from the air molecules themselves, referred to as Rayleigh scattering. Ozone plays an important role in the light absorption mechanism but at lower wavelengths (<330 nm). Mie scattering is strongly related to aerosol concentration in the atmosphere and varies significantly at difference location and times. Typically, aerosols are concentrated in the lower part of the atmosphere. The scale height for aerosol particle concentration is on average 1.2 km, with a mean free path of 14 km at 360 nm. In the upper atmosphere, the scattering of the light is almost entirely governed by the Rayleigh scattering. The angular dependence $\mathbf{d\Omega/d\vartheta}$ is proportional to $\mathbf{(1+\cos^2\vartheta)}$. The exponential attenuation length at sea level is about 24 km and its path length increases proportionally to λ^4. The total transmission factors for light propagating from a point source to a receiver can be expressed as:

$$T=T_{Rayleigh}+T_{Mie}+T_{Ozone} \tag{2.13}$$

where the Rayleigh transmission factor[14] is given by:

$$\ln (T_{Rayleigh})= - x_0/X_R \; |(\exp(-h_1/H_0)- \exp(-h_2/H_0)| \; (400/\lambda)^4 \cdot \sec\vartheta \tag{2.14}$$

with:
x_0 the vertical depth at the observation level (x_0=1030 g/cm^2 at sea level);
X_R the mean free path at sea level and at 400 nm (X_R=2970 g/cm^2);
h_1 and h_2 the source and receiver heights in km;
H_0 the atmosphere scale height (H_0=7.4 km at sea level);

λ the wavelength in nm;
ϑ the slant depth angle between source and receiver location;

and the Mie transmission factor[14] is:

$$\ln (T_{Mie}) = H_M/L_M \, [\exp(-h_1/H_M) - \exp(-h_2/H_M)] \cdot \sec \vartheta \qquad (2.15)$$

with:
H_M the Mie scale height (H_M=1.2 km);
L_M the Mie scattering mean free path at 360 nm (L_M=14 km typically);
$h_1 > h_2$ the source and receiver heights in km;
ϑ the slant depth angle between source and receiver location;

and finally the Ozone transmission is given by:

$$\ln (T_{Ozone}) = -\mu(\lambda) \cdot \mathbf{X} \qquad (2.16)$$

with:
$\mu(\lambda)$ extinction coefficient ($\mu(\lambda)=10^{113.4-44.21\log(\lambda)}$ cm^2/g);
X Ozone thickness ($X= 4 \cdot 10^{-4}$ g/cm^2);
λ the wavelength in nm.

Atmospheric monitoring is a fundamental task in any experiment using the air as active detector. Careful measurements of light attenuation should reduce the uncertainty on the atmospheric transmission to the level of a few percent.

2.5 Reflection/diffusion on rough surface: qualitative considerations

To determine the light scattered by a generic surface (no absorption is considered in this discussion), three parameters must be considered: the wavelength of the light, its angle of incidence and the surface roughness. Specular reflection changes into diffuse scattering according to the values of these parameters, as suggested by the Rayleigh criterion[15]. Figure 5 shows the geometrical derivation of the Rayleigh criterion. Consider rays **A** and **B** incident on a surface with irregularities of height **h** at an incident angle α. The path difference between the two rays is:

$$\Delta l = 2h \cdot \sin \alpha \qquad (2.17)$$

with a phase difference of

$$\Delta\varphi = 2\pi \cdot \Delta l/\lambda = 4\pi \cdot h \cdot \sin \alpha/\lambda \qquad (2.18)$$

If this phase difference is small, the two rays will be almost in phase as they are in the case of a perfectly smooth surface. If the phase difference increases, the two rays will interfere, until for $\Delta\varphi=\pi$ they are in phase opposition and cancel. If there is no energy flow in this direction, then it must have been redistributed in other directions, as it cannot have been lost. Thus, for $\Delta\varphi = \pi$ the surface scatters and hence it is rough, whilst for $\Delta\varphi = \mathbf{0}$ it reflects specularly and it is smooth. The right side of (2.18) thus gives:

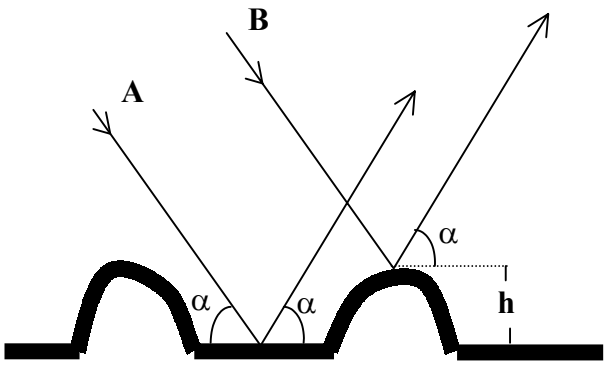

Fig. 5: Derivation of the Rayleigh criterion.

$$4\pi \cdot h \cdot \sin\alpha/\lambda \tag{2.19}$$

as a measure of the effective roughness of a surface. A surface will tend to be effectively smooth under two conditions:

$$h/\lambda \to 0 \quad \text{or} \quad \alpha \to 0. \tag{2.20}$$

Conventionally a surface is considered smooth for

$$h < \lambda/(8\cdot\sin\alpha) \tag{2.21}$$

corresponding to a value of $\Delta\varphi = \pi/\mathbf{2}$. Often $\pi/\mathbf{4}$ or $\pi/\mathbf{8}$ are found in the literature as more realistic values for $\Delta\varphi$. When the irregularities of the reflecting surface are very large compared to the wavelength, diffuse scattering turns into isotropic scattering. This is the case for the Cherenkov light impacting the Earth surface, for which isotropic scattering will be assumed hereafter.

2.6 Background

Night sky UV light background, with and without Moon, has to be known in order to discern the signal from random fluctuations due mainly to scattered light from the stars, photochemical processes in the Earth atmosphere and man-made light sources. Previous background measurements at mountain altitude (1.6 km) give as average intensity of background $\mathbf{<B>} \sim 400$ photons/(m^2 ns sr) in a moonless night. This value increases by a factor larger than 10 in presence of full moon. The number of photoelectrons generated by the background light in a photo-sensor can be estimated as follows:

$$N_{bk} = <B> \cdot \varepsilon_{tot} \cdot A \cdot \Delta\Omega \cdot \Delta t \tag{2.21}$$

where ε_{tot} is the total efficiency of the optical detection unit (including PMT quantum efficiency, filter transmission, collecting efficiency, geometrical inefficiency), **A** is collecting area, $\Delta\Omega$ the solid angle subtended by the photo-sensor and $\Delta\mathbf{t}$ the signal gating time. The fluctuation of this number represents the noise present during the reception of an event.

Locating the apparatus away from man-made light sources should eliminate most of the uncorrelated noise, often source of fake triggers, and increase the signal to noise ratio.

3. ATMOSPHERIC PHENOMENA: METEORS

3.1 Overview and general information

The Earth, with its atmosphere, is exposed to a continuous inflow of material objects (meteoroids) from the interplanetary medium; in reality this inflow results from the apparent motion of the objects when encountered by the Earth in its orbital motion. Meteoroids, ranging in diameter from microns to meters, meet the atmosphere of the Earth at a speed extending from ~ 10 to ~ 70 Km/s, dissipating their kinetic energy by friction driven processes with ablation and energy transfer to the air molecules. Associated to the meteoroids and phenomenologically similar, are the orbital debris, artificial environment made of orbiting particles, leftover pieces from non-operational spacecrafts, boost stages, solid rocket fuel particles, and other man-made space objects. Meteoroids and orbital debris interact with the atmosphere both through macroscopic scale phenomena (e.g. emission of electromagnetic radiation, heating, ablation, fragmentation, etc.) and microscopic scale phenomena (excitation and dissociation of molecules, excitation and ionization of atoms, thermal and mechanical emission of electrons, etc.). The term “meteor” refers to the source of electromagnetic radiation associated with the meteoroid/debris as a consequence of its interaction with the atmosphere; the radiation covers all wavelengths although conventionally the name meteor refers to the observation band in the optical/visual range.

EUSO, conceived with the main scientific objective of investigating EECR by detecting the UV fluorescence induced in the atmosphere, has characteristics of sensitivity, spatial resolution and high sampling rate which enable the disentangling of UV light produced by Cosmic Rays (“fast” signal) from that due to other phenomena such as meteors, lightning, atmospheric flashes (“slow” signal). EUSO is foreseen to produce valuable information on the meteor field, extending the observation range to very low luminosity and very high sampling rates[1)]. The observation of meteors complements the EUSO cosmic ray related science objectives. Meteor observation in the UV with the very high sensitivity and sampling frequency typical of EUSO will allow the search for matter distribution otherwise unobservable in the vicinity of Earth and the investigation of interaction processes at very high Mach number not accessible in ground based experiments. EUSO is expected to shift the limiting magnitude for observation from 6 (direct vision) to about 18 with a gain of the order of 10^5 in Brightness.

3.2 Detection in ULTRA

The "EUSO meteors" study for Phase A requires observations from ground. These, in turn, demand an appropriate Visible/UV optical intercalibration and a contextual verification of simulation data. Ground observations of meteors can be accomplished with minor efforts by taking advantage of already existing instruments/facilities like BABY and ULTRA. The instrumentation, in fact, is basically the same used for the observation of the diffuse UV background (**BABY**) and the Cherenkov reflected/diffused (**ULTRA**).

The Specific “Meteor” Requirements for ULTRA can be summarized as follow:

1. A special mode of operation needs to be introduced for the electronics and memory storage to take into account the different time range of EAS and Meteors.

The "*Residence Time on a Pixel*" and the "*Duration"* of a generic meteor phenomenon are, when compared to EAS, of the order:

$$\frac{Time_{Meteor}}{Time_{EAS}} = 10^4 - 10^5$$

2. The Field of View needs to be extended to ± 30^{o} in order to include a substantial fraction of the meteor track (reference values are 50-100 km track length at 100 km height with 45^{o} entry angle). This of course has to be traded in agreement with the characteristics of the photomultipliers (constrains given by background or possible saturation during the observations etc..)
3. Possibility of a contextual observation of the meteors in the optical range in order to validate and calibrate the results of the observations in UV.

As a practical conclusion, Meteor observations can be made from the same location of ULTRA employing the same basic instrumentation and the same Team. The same observation campaigns can be shared exploiting the same logistic and support.

4. ULTRA OBJECTIVES AND DESCRIPTION

The Ultra apparatus is a hybrid system consisting of an UV optical detection unit, the UVscope, and an array of scintillators, the ETscope (EAS Telescope). The Uvscope is used to detect Cherenkov reflectively diffused UV light from EAS which are detected in coincidence by the ETscope array. Data taking and synchronization between the UVscope and the ETscope is performed by radio-link using commercial available wireless technology and GPS (Global Position System) devices. A LASER system is used to characterize the atmosphere in the measurements of Cherenkov reflected/diffused light and as an essential tool for the determination of the reflection coefficient and hence the expected albedo from clouds.

The main objectives of the ULTRA experiment can be summarized as follows:

- Detection of the Cherenkov light associated with EAS:
    - Measurement the average reflection/diffusion coefficient of different surfaces:
        a) Grass-covered land
        b) Trees-covered land
        c) Uncultivated land (desert)
        d) Iced land
        e) Water-Sea
    - Measurement of the reflection/diffusion coefficient as a function of the shower axis inclination for the characterized surfaces.

Observations in different location will obviously be needed to achieve these goals. As first site we propose the Mont-Cenis lake shown in the Figure 6, where surfaces a), d), and to some extent e) are present. Moreover the proposed site is locate at ~ 2000 m above sea level (a.s.l.), increasing considerably the EAS trigger rate.

- Measurement of several atmospheric parameters under different conditions:

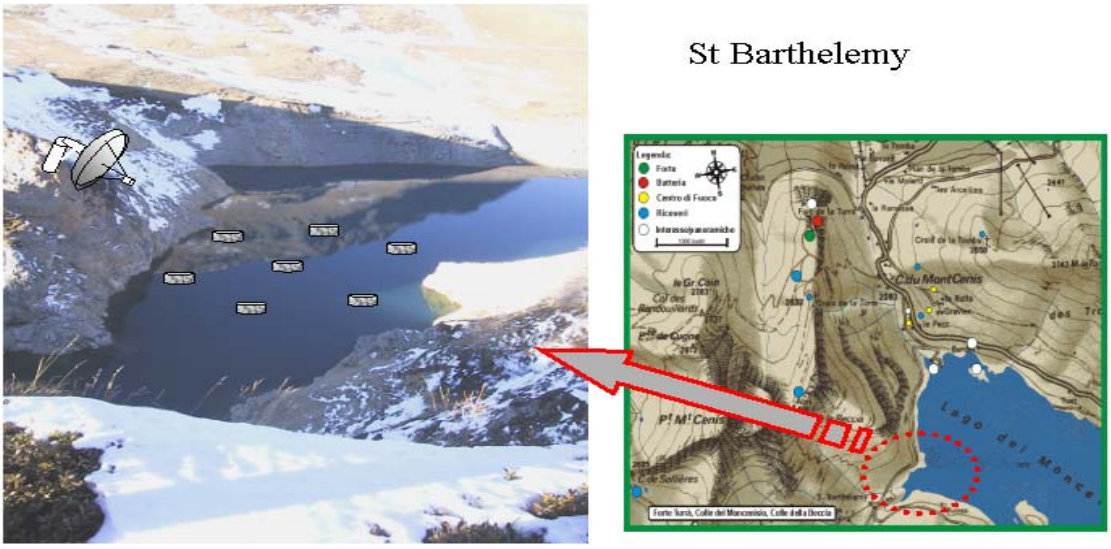

Fig. 6: Pictorial view of the ULTRA experiment on the Mont-Cenis lake.

- Measurement the UV diffuse background at different Moon phases
- Study and determination of the atmospheric attenuation at different detector heights
- Measurement of the reflection/diffusion coefficient in the presence of clouds

- Meteor observation:
  - Preliminary measurement of meteors UV light
  - Validation and calibration of the UV yield with contextual observation in the optical range.

In order to achieve these objectives an accurate and consistent interpretation of the data is necessary. An efficient identification of spurious signals (for example laser multiple returns) is crucial. Specific software tools for analysis and archiving of the experimental data will have to be developed.

4.1 The UVscope

The UVscope consists of four Hamamatsu R3878 photomultiplier tubes (PMT). This type of PMT has a bialkali photocathode of 8mm of diameter and an UV transmitting glass window. The PMT has 8 dynodes and a typical gain of the order of $3 \cdot 10^5$ at 1200 V. Each tube is mounted inside a cylindrical aluminum case and can operate in single photoelectron counting and/or charge integration mode. All the power supplies are embedded inside the aluminum case together with the related electronics. A light collimator is also used to regulate the angular aperture of the detector and contemporarily protect from stray light the PMT sensitive area. Each of the UVscope detector unit allows different filters and converging lens to be accommodated on the top of the collimator in front of the PMT cathode. Figure 7 shows the sketch of one UVscope unit. Each unit, holding a PMT, can be daisy-chained with other units and through a parallel bus connected to a PC.

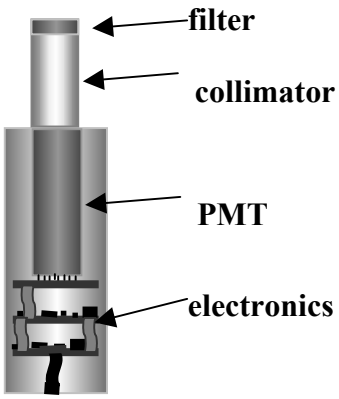

Fig. 7: The UVscope unit. Artist view of the main elements and their location inside the aluminum case.

Each UVscope unit can operate independently and data acquisition is performed on-line with all the detector functions fully monitored and controlled by an on-site computer system. A scheme of the electronics is shown in figure 8. The front-end exhibits a double pulse resolution better than 10 ns allowing for single photoelectron counting. Charge integration can be performed at 10 MHz. Memory buffers assure a fast storage of the relevant digitized counting/charge data. Dumps of the data from the different channels on the local PC hard disk are performed at a given rate under the control of the UVscope real time acquisition software.

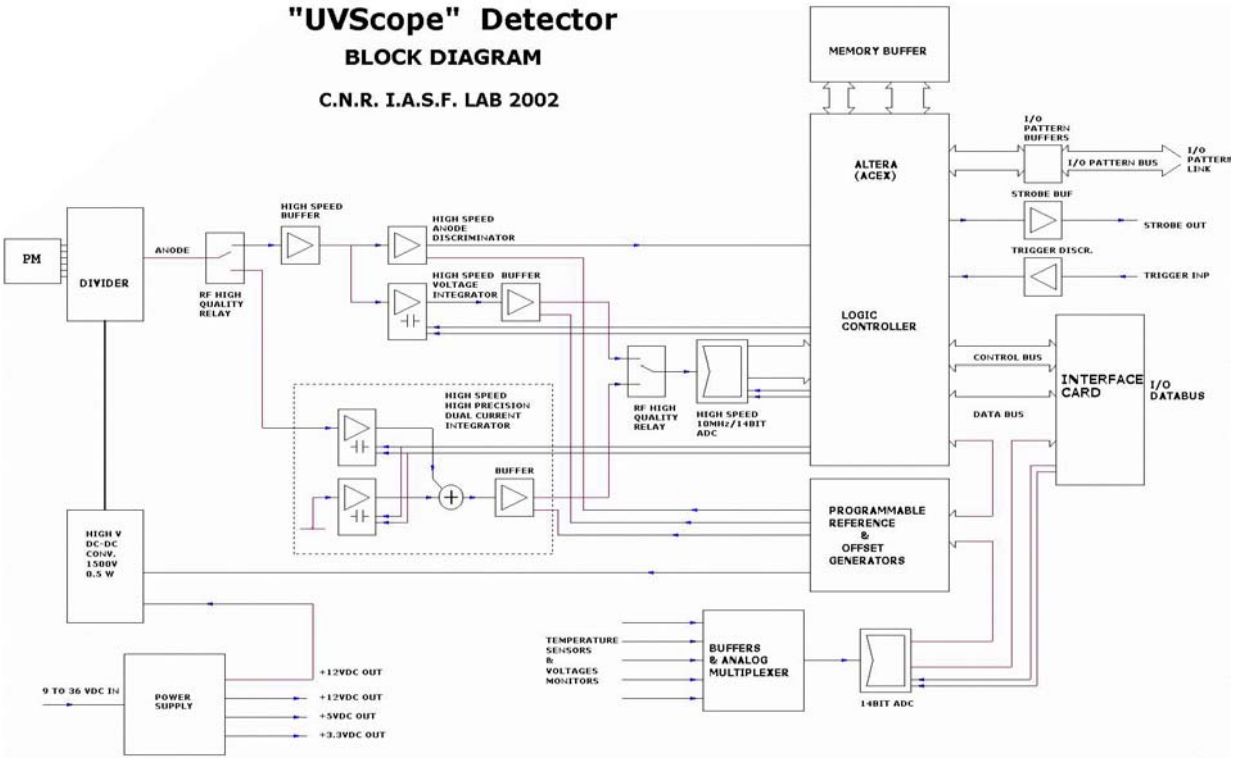

Fig. 8: Block diagram of the electronic of a UVscope unit.

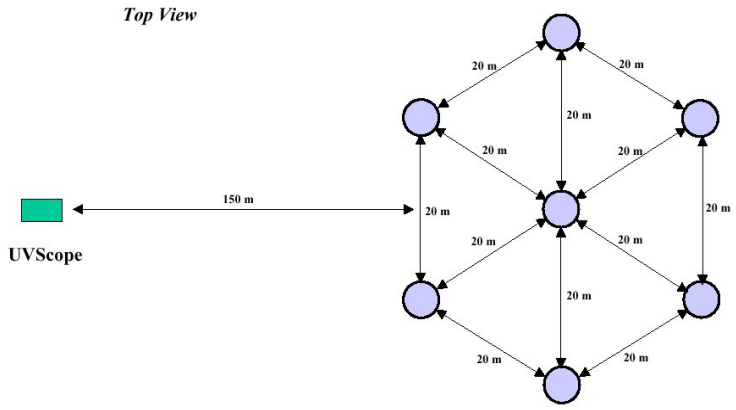

Fig. 9: Top view of the ETscope setup.

4.2 The ETscope array

The ETscope consists of 7 (+ 1 spare) stations suitable to detect the electromagnetic component of EAS. An efficient geometrical arrangement of the ETscope is shown in figure 9. Each detector consists of a plastic scintillator NUCLEAR NE 102A with dimensions 80 x 80 cm^2, 4 cm thick. The scintillator is seen by two photomultipliers Philips Photonics XP 3462B in coincidence, the photocatode diameter being 68 mm. For a power supply HV = 1.8 KV the gain is $5 \cdot 10^6$ and the current is ~ 0.5 mA with the high gain voltage divider A[16]. The scintillator is housed in a pyramidal box with 86 x 86 cm^2 base and the photomultipliers placed on the top with the photocathode at a distance of 28.5 cm from the scintillator surface as shown in the figure 10. The box is internally coated with white diffusing paint; direct and reflected light is collected on the photocathode. With these specifications the light yield is ~ 40 p.e./m.i.p. at the quoted gain, with saturation at ~ 40 m.i.p./0.64 m^2. Since EUSO will observe mainly water (~ 70% of the Earth surface is covered by the oceans), it is very important to perform the measurement on a sea or lake surface. For this reason the detector,

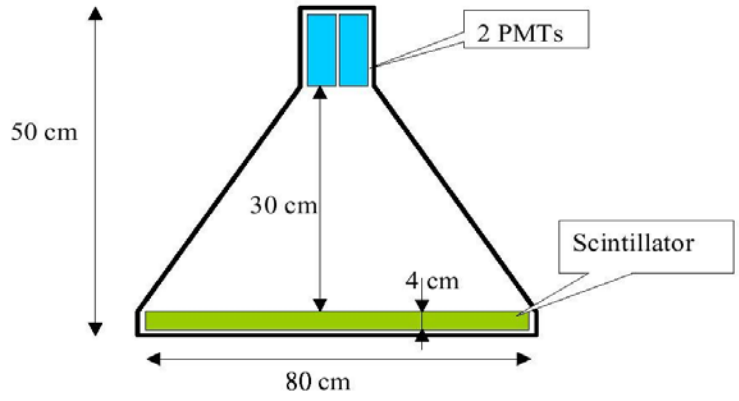

Fig. 10: Schematic view of one ETscope detector.

together with the electronics, batteries and DAQ, is housed in a waterproof box. For the same reason the array units, made by independent counters, are able to record and send acquired data by means of radio-link to a receiver center.

4.3 LASER description

A Q-switched Nd-YAG Laser is used to complement and support the specific measurements of ULTRA. The ULTRA Laser operates in the 1064 nm, 532 nm and 355 nm wavelength. The main technical characteristics of the Laser can be summarized as follows:

•Pulsed light of 5 ns @ 20 Hz
•Energy 30 m J @ 532 nm
•Beam divergence of 1.5 m radian

The laser system is easy to transport (20 kg) and operate. A cabinet and a head form it. Air-cooling system (water/air heat exchanger) assures open field operation and transportability. The Laser is equipped with synchronization and control electronics that allows laser beam synchronization by external trigger and PC remote control.

4.4 Position determination and time synchronization

An EAS will be detected in ULTRA by the coincidence of the seven scintillator detectors constituting the ETscope. Depending on the type of surface, the scintillators could be either at fixed positions (ground) or moving (water). In order to allow the foreseen measurements, each element of the ETscope array should be equipped with a position determination system. The determination of the shower arrival direction requires precise time synchronization between the array elements.

Position determination

To achieve relative position accuracy better than 1m at velocities up to 3m/s an approach using GPS devices is under study. The receiver under test is a Motorola Oncore M12. The manufacturer specifies a precision of 25 meters for absolute position determination. In the ULTRA experiment the receiver will be used in differential mode. In this mode one receiver is used as a reference. In this case a cancellation of systematic errors of absolute position determination of the scintillators array (receivers working in scheduled common view) is obtained. The expected accuracy of the relative position determination for the M12 is of the order of 30 cm.

Synchronization

Relative timing precision better than 10ns is required to synchronize the ETscope units. A system based on relative time measurement is under development (Time-Tagging System).
The Time-Tagging system is composed by several units, one per station, and must time-tag each event in each station. The time-differences between the several events in the several stations are computed offline thus allowing to trigger on EAS and to reconstruct the arrival direction.
Each unit includes a low-cost, commercial GPS receiver (GPSboard) to coarse time-tag and custom electronics (TMS – Time Measuring Subsystem) to perform the fine time-tagging.

The GPS board generates a pulse that marks the UTC seconds (PPS). The identification of the second (year, month, day…) is provided through a RS-232 protocol. The absolute accuracy of the PPS, stated by the manufacturer, is of the order of 40ns. This error is mainly due to the inaccurate knowledge of the propagation of signals from the GPS satellites to the receivers, namely the propagation in the atmosphere under the different atmospheric conditions. Nevertheless, since the stations are near, it can be assumed that the propagation conditions are the same for all the receivers and the errors involved can be viewed as systematic errors that cancel when taking time differences. The relative accuracy has been measured to be better than 3ns for the receivers used[17].
The TMS measures the time between the PPS and the local event trigger. TMS also measures the time between consecutive PPS pulses for calibration purposes. Preliminary tests performed on the TMS indicate a precision better than 5ns.
The absolute time of an event in a station is the sum of the time of the previous PPS, given by the GPS, with the time measured by TMS. The total error is therefore the convolution of the GPS error with the TMS error. It is foreseen a full test on the time-tagging system to estimate the global accuracy of the system and that should be of the order of 5ns.
The description of the TMS implementation is presented in the next section.

4.5 Data acquisition and telemetry

A) UV Scope

Each of the four detectors of UVscope operates in continuous-acquisition mode. The single photoelectron signal from anodes is digitally added to the counters and/or contribute to the charge amount collected in the integration section. The energy information (counters/charges) and the related time are stored into the on board memories (1Mbyte) at each appreciable variation. The memory is divided in 2 banks: while the first is accumulating data from "inputs" the second is transmitting stored data to a mass memory unit (PC hard disk/telemetry) and vice-versa. The acquisition time unit is limited to no less than 100 ns for integration (10 MHz ADC) and to no less then 10 ns for counting (memory write cycle = 10 ns, digital resolution = 4 ns). A 100 ns interval is the fast acquisition time unit allowed. In this case, the uninterrupted sequence before data transfer should be no more then 25ms (4bytes*256k*100ns = 25ms ⇒ 40Mbytes/s). This time interval is programmable allowing

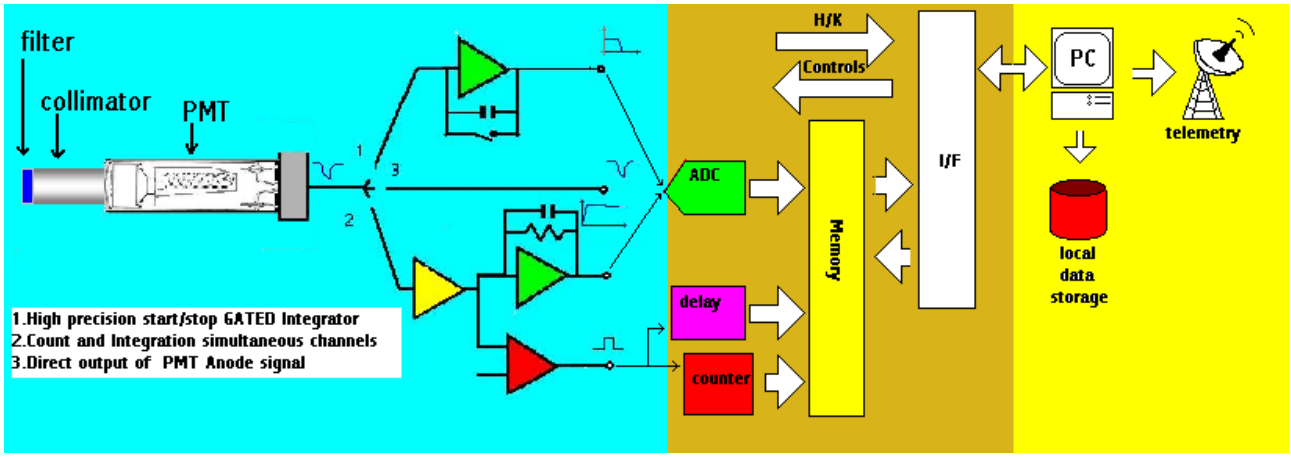

Fig. 11: Uvscope general working scheme.

different acquisition times longer than 100 ns.
Housekeeping data will be inserted in memory at a slow rate and transmitted in turn by telemetry.
Only relevant information, for example count/charge integration mean values per second and so on, will be transmitted by telemetry. Figure 11 shows the general operational scheme.

UVscope Functional Requirements

- For each unit the DAQ system shall:
  - digitalize the analog signal of the PMT anode corresponding to one p.e. (single photon counting) with 10 ns double pulse resolution;
  - digitalize the analog signal of the PMT anode (charge integration) in 100 ns (limit of the adopted ADC);
  - record the digitalized data, if different from the previous one recorded with the related time;
  - monitor the housekeeping and statistical data;
  - provide and control the high voltage bias, threshold and offset for the PMT;
  - provide sync signals for test and calibration.
- Operational Requirements
  The DAQ system shall be able to:
  - operate autonomously without manned contribution once powered on;
  - run all the acquisition software tasks simultaneously: PMT charge and time, position, temperatures, high voltage control and telemetry management;
  - operate without failures for at least a nocturnal acquisition;
  - mass storage autonomy compatible with the acquisition time set.
- Interface Requirements
  The DAQ system shall:
  - be powered with on-board batteries;
  - send data and receive command from the telemetry system;
  - receive and use time reference signal from a GPS system;
  - receive data from a GPS system;
  - operate with a sufficient throughput to record the scientific data.
- Environmental Requirements
  The DAQ system will be able to operate:
  - within the following temperature range: -10°C to +40°C;
  - in open field and humid environment.

B) ET Scope

For every event on each station the energy deposited in the scintilator and the arrival time shall be estimated. Coincidences among different detectors are then found off-line, using the arrival time of each unit. Since the expected single counting rate at sea level is ~ 180 Hz/m^2, the contamination by random coincidences will be negligible.

The acquisition system is based on a board developed at LIP (LIP-PAD board) that is able to perform time-tagging of events and that is also capable of digitizing PMT signal and digitally trigger on events.

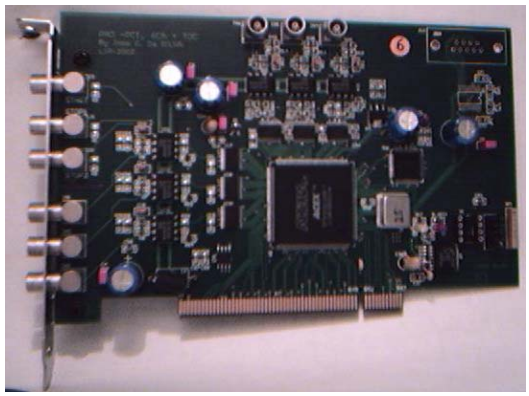

Fig. 12: Photograph of the LIP-PAD board.

The LIP-PAD board is a PCI based acquisition board and is constituted by an Analog Acquisition Subsystem (AAS) and a Time Measuring Subsystem (TMS) that with the GPS board constitute the Time-Tagging system.
The LIP-PAD is composed of three main blocks:

- the AAS features 6 analog acquisition channels, each of which is composed by a shaper, an amplifier and a 10 bits flash ADC of 100MHz. An onboard memory and a digital trigger unit are also part of the AAS and are common to all channels;
- the TMS is composed by a TDC and a 32 bit counter running at 50MHz;
- a control and readout with a PCI interface.

The digital units are implemented on a PLD in which, by reprogramming, logic units can be easily modified, e.g., the trigger modes can be easily changed.
In the AAS the analog signals are shaped, amplified and then digitized by the ADC. The ADC samples the signal voltage with a frequency of 100MHz and writes the values to a buffer memory. The digital trigger unit can implement various trigger conditions (e.g. simple threshold, muon, double pulse, shower). On trigger the buffer memory and consequent data is saved on memory and read by the PC through the PCI bus. The total amount of data recorded is defined on the PLD and is, to this date, of 256 positions. This means that 2.6 μs of data is recorded.
The position of the trigger in this interval is defined in the DAQ software (from 0 to 256). Choosing the middle value allows having a 1.3 μs data before and after the trigger. Thus trigger generation does not assume such a crucial role as in charge integration acquisition systems that require a precise interval for integration, built from trigger. The analysis software must be able to select the relevant data of an event and extract the important parameters of the signal, such as the area that corresponds to the charge, which is proportional to the deposited energy on the scintilator.

The TMS is responsible for the measurement of the time difference between the synchronization pulse, from the GPS board, and an event.
The system developed consists of a clock (50 MHz oscillator and counter) combined with a TDC. The use of a clock allows the 1s dynamic range while the use of a TDC allows the precision necessary without having a 1GHz frequency oscillator. The oscillator period is calibrated with the signal from the GPS.

Preliminary tests were already performed and indicate that the TMS has a precision better than the specification required.

The distributed DAQ system to be used in ULTRA consists of several PCs (one per station, equipped with a LIP-PAD board, a GPS, a wireless data transmission system and a HV power supply. DAQ must be able to:

- record or transmit the arrival time detection of each trigger signal with less than ±5 ns of accuracy to the Central Control & Communications Point (CCCP);
- record the absolute position of each station with a 1m precision;
- provide and control the high voltage bias for the 2 PMTs;
- send controlled DC voltage to the high voltage DC/DC converters;
- measure temperature with sensors disposed in the station;
- be powered with on-board batteries;
- send data and receive command from CCCP;
- have a maximum trigger rate of the same order of the single counting rate.

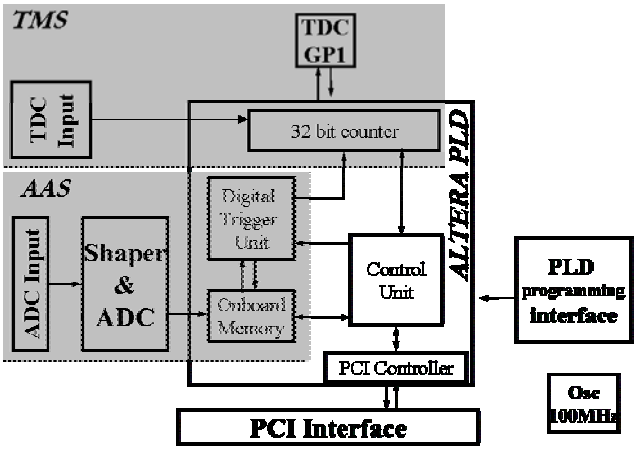

Fig. 13: Block diagram of the LIP-PAD board.

5. ULTRA GEOMETRY AND DESIGN PARAMETERS

The ULTRA apparatus operates in open field environment and requires a suitable site allowing a convenient geometrical set-up. Moreover, low man-made light sources contamination and clear nights are required in order to disentangle Cherenkov light pulses from night sky background. Figure 14 shows a favorable geometry for running the experiment. The UVscope is placed on the top of a hill whereas the ETscope array is located on the valley. The field of view of the UVscope is oriented in such a way that the UVscope detectors image the overall scintillator array.

The combined operation of UVscope and ETscope allows the detection of reflectively diffused light from the EAS landing inside the area sampled by the scintillator array. Moreover, ULTRA uses a Laser for continuous monitoring of the atmosphere transmission during the running periods.

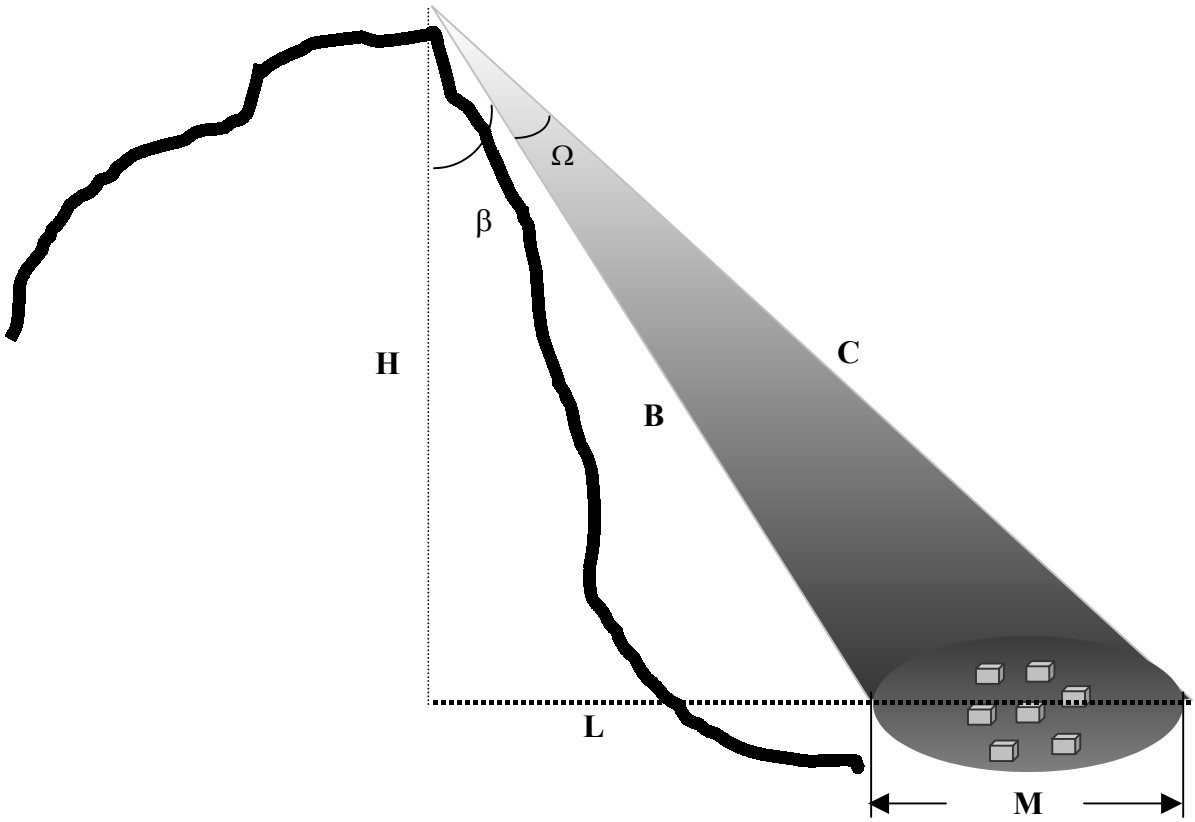

Fig. 14: Sketch of a typical configuration for the detection of Cherenkov light reflectively diffused by EAS. The gray ellipse represents graphically the coincidence area shared by the UVscope and ETscope array.

The following subsections treat separately the detection techniques of the UVscope and the ETscope array. Also, they discuss and implement the preliminary calculations needed to identify the experimental parameters relevant for the measurements.

5.1 UVscope detection parameters

As stated in section 4, the UVscope consists of four PMT that can operate in single counting mode and/or in charge integration mode. The four PMTs are used in stand-alone or cluster configuration, depending on the specific requirement of each measurement. In this section the general detection technique of one UVscope unit is described, inferring the same for the other units. Although complete Monte Carlo simulations will have to be carried out to include all the relevant elements affecting the measurements, some basic calculations are useful to define the main parameters involved and improve the performance of the apparatus. In particular, the relation between the signal to noise ratio and the geometrical parameters of the detection system is derived in a few practical cases, for illustrative purposes.

As a starting point, it is necessary to identify the essential parameters that define the experiment. It is assumed that the Cherenkov light pulse in an UVscope unit results from the reflectively diffused signal of the UV Cherenkov photons belonging to the EAS. The characteristic light "pool" of the Cherenkov radiation is shown in figure 15 and it describes the lateral distribution function (LDF) for Cherenkov light from a shower of energy 10^{16} eV. In the figure, it is visible the existence of a relatively flat plateau, up to distances from the

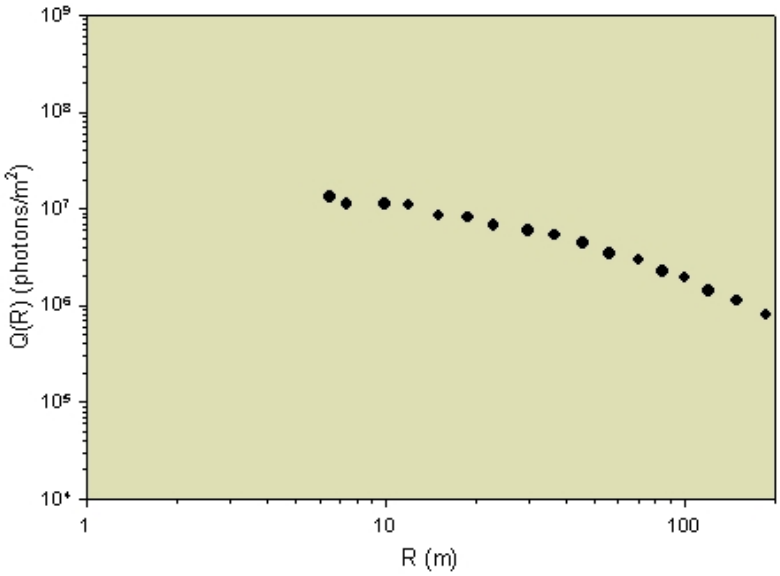

Fig.15: Lateral distribution function of Cherenkov photons for a proton of $E = 10^{16}$ eV.

shower core of the order of 200 meters. Fitting the LDF experimental data points of figure 15 with a rational equation of two parameters of the form Q=a/(1+bR) is the first step to deduce a parameterization formula. From the parameterized LDF, the integrated number of photons inside the Cherenkov pool of radius $\mathbf{R_p}$=200 m was calculated for the chosen primary energy. In order to evaluate the expected signal in each of the Uvscope units, the full field of view angle Ω (see Figure 14) has to be determined. From figure 14, a simple relation between the β and Ω angles can be extracted:

$$M/\sin\Omega = C/\cos\beta \tag{5.1}$$

Using this relation and still referring to the figure 14, it is straightforward to show that the full field of view Ω can be written as a function of **H** (the vertical height at the UVscope location), **M** (the diameter of the area imaged by the Uvscope) and **L** (the horizontal distance from the UVscope vertical projection to the imaged border) :

$$\sin\Omega = H \cdot M /(X \cdot Y)^{1/2} \tag{5.2}$$

where $\mathbf{X= (L+M)^2+H^2}$ and $\mathbf{Y=L^2+H^2}$. Figure 16 shows the relation of **L** and **H** to Ω, fixing **M** to a value of 120 m. The expected total signal from a surface of diameter **M** at the position **H** of the UVscope unit depends on the shower zenith angle and can be calculated in terms of total number of detected photoelectrons as:

$$N_{pe} \approx P_c \cdot T(\lambda) \cdot R \cdot A \cdot \varepsilon_{tot}(\lambda) \cdot \cos\theta \,/(2 \cdot \pi \cdot r^2 \cdot S) \tag{5.3}$$

where $\mathbf{P_c} \approx 3 \cdot 10^{11}$ is the total number of Cherenkov photons (for shower energy of 10^{16} eV) integrated in a circle of radius $\mathbf{R_p}$, λ is the wavelength, $\mathbf{T(\lambda)}$ is the atmosphere transmission coefficient, **R** is the reflection coefficient, **A** is the collecting UVscope collecting area, $\varepsilon_{tot}(\lambda)$ is the total detector collecting efficiency including lens transmission, detector Q.E. and filters

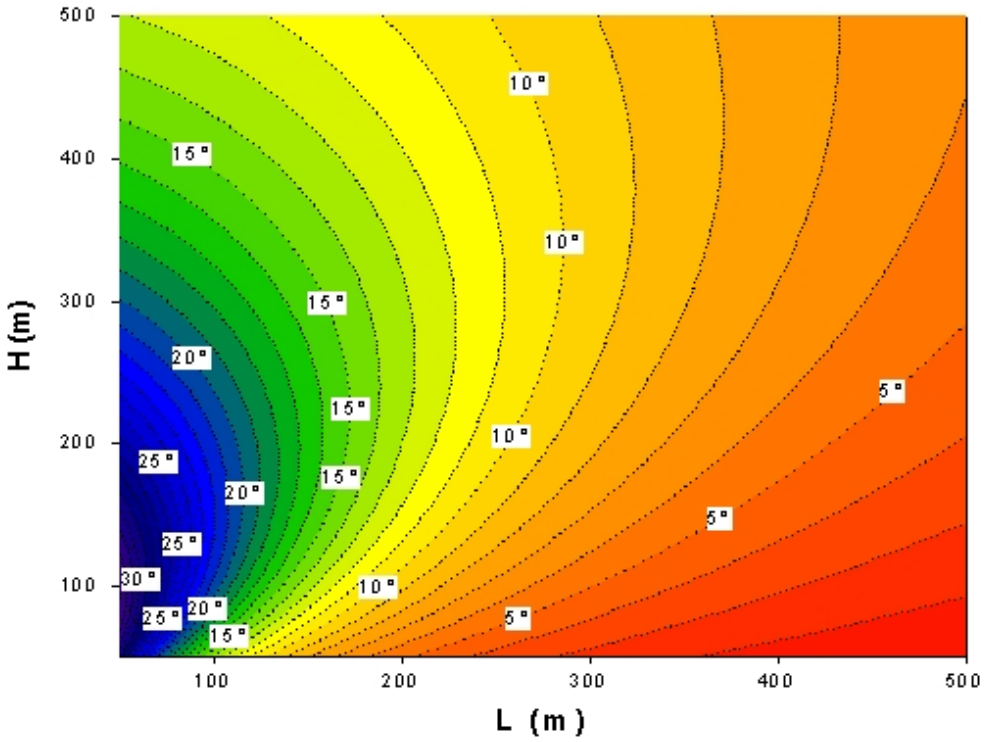

Fig. 16: The full FOV angle vs H and L. The diameter M of the imaged area has been fixed to 120 m.

transmission, θ is the EAS zenith angle, **r** is the average distance between the UVscope detector and the center of the ETscope array and finally **S** is a correction factor that takes into account the active fraction of the monitored area and is defined as $\mathbf{(2\cdot R_p/M)^2}$.
An estimation of the pulse duration and shape expected on the UVscope detector as a function of the shower zenith (θ**)** and azimuthal (φ**)** angles and of the FOV Ω can be obtained on the basis of purely geometrical considerations. The pulse duration $\Delta\mathbf{P_t}$ it is given by:

$$\Delta P_t = (S_{t1} + S_{t2})/c \tag{5.4}$$

where $\mathbf{S_{t1}}$ is the perpendicular distance of the points (where Cherenkov photons will arrive) of the imaged area to the shower front plane:

$$S_{t1} = [M/2- (x_r \cdot \cos\varphi + y_r \cdot \sin\varphi)]\cdot \sin\theta \tag{5.5}$$

and $\mathbf{S_{t2}}$ is the distance of the Cherenkov photons of the imaged area to the UVscope detector site:

$$S_{t2} = [(L + M/2 + x_r)^2 + y_r^2 + H^2]^{1/2} \tag{5.6}$$

Finally, replacing (5.5) and (5.6) in (5.4):

$$\Delta P_t=1/c \cdot [M/2- (x_r \cdot \cos\varphi + y_r \cdot \sin\varphi)] + [(L + M/2 + x_r)^2 + y_r^2 + H^2]^{1/2}\cdot \sin\theta \tag{5.7}$$

where **c** is the velocity of light, $\mathbf{x_r}$ and $\mathbf{y_r}$ are the position coordinates of the Cherenkov photons on the imaged area.

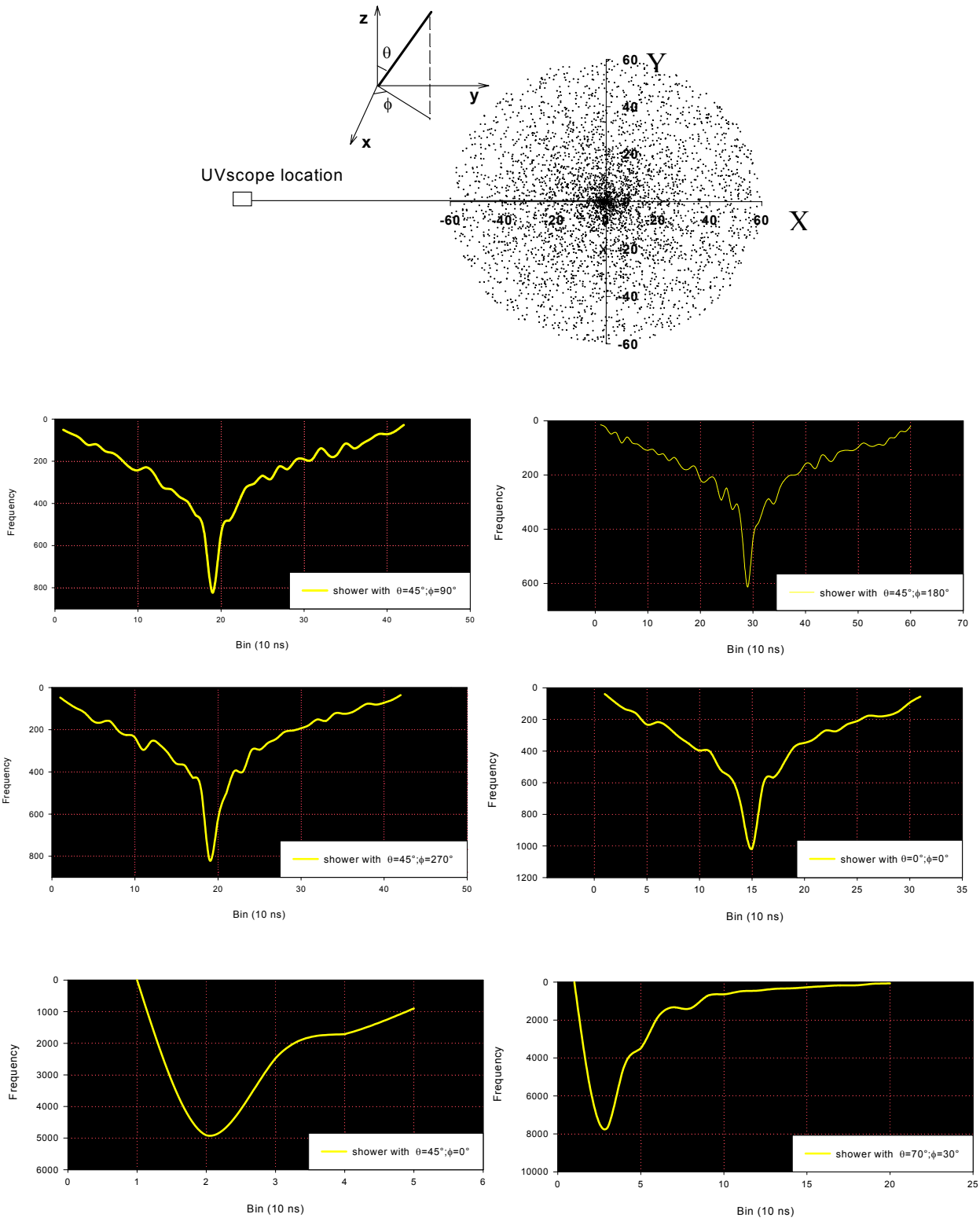

Fig. 17: The top figure shows the combined UVscope and ETscope geometry. Simulated Cherenkov photons positions are also shown. The graphs of simulated time and shape profiles are shown for events with different values of zenith (θ) and azimuth (φ) angle.

Some examples of expected pulse duration and shapes at the UVscope location are shown in figure 17 using a simple Monte Carlo program developed for this purpose. As expected, the

signal profiles depend strongly on the combined geometry of the shower directions and UVscope location.
Within these simplifying assumptions, it is interesting to establish, in a practical case, the performance of the UVscope detector in terms of signal intensity and signal to noise ratio.

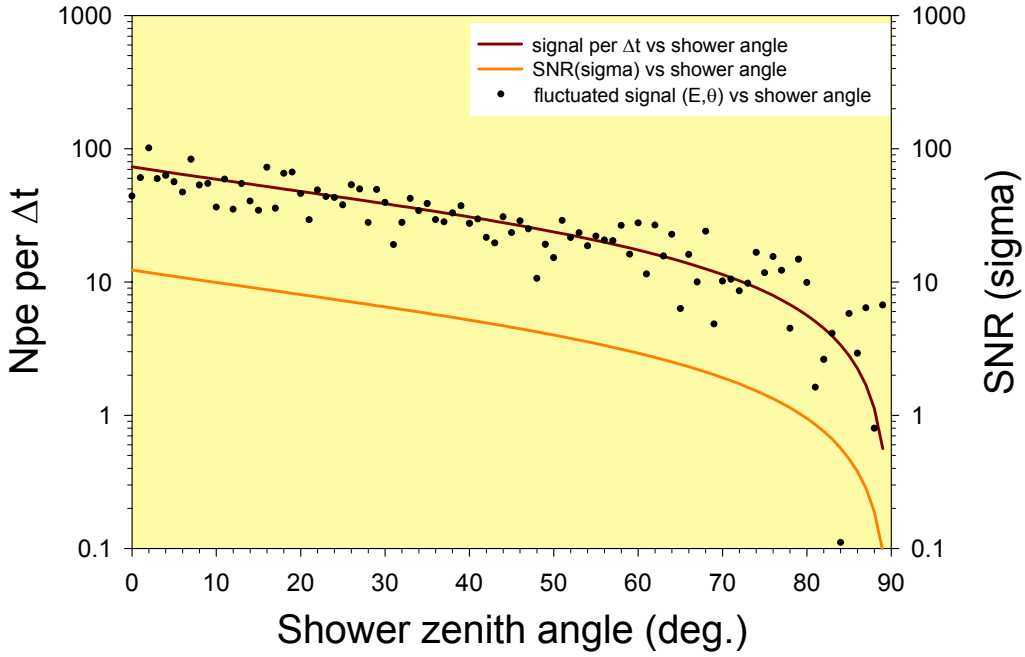

Fig. 18: UVscope expected performance for the practical case described in the text.

From equations (5.2), (5.3), (5.4) and (2.13) and assuming a total detector efficiency $\varepsilon_{tot}(\lambda)=0.1$, atmospheric transmission and reflection coefficients of T=0.8 and R=0.1, a detector collection area $A= \pi \cdot (75 \cdot 10^{-3})^2$ m^2 , a Cherenkov radius pool R_p=200 m, and an average background <B>=500 photons/ns/m^2/sr it is possible to calculate the signal to noise ratio and signal intensity as a function of the shower zenith angle θ. Figure 17 shows the expected reception performance of a UVscope unit fixing L =75 m, H=100 m, M=120 m and with a gate integration time Δt of 100 ns sampling the pulse duration ΔP_t given by equation (5.7).
The scattered points of figure 18 represent the amount of the dispersion of the signal when the error in determining the shower energy and zenith angle are included. For the examined case a ± 20% in energy resolution is adopted while an 8° error is introduced in the determination of the shower arrival direction. It is important to note that for angles less than 45°, a practical value for EAS scintillator arrays, the sensitivity of the UVscope detector is, in terms of signal to noise ratio (SNR), greater than 5 σ.

5.2 ETscope array detection parameters

The Etscope will trigger on EAS and measure their shower size and arrival direction.
The shower size is obtained minimizing the NKG lateral distribution of EAS (2.5) to the particle density in each detector (derived from the measurement of the energy deposited in the scintillator). This procedure requires the determination of the core location, i.e. the position of

the shower axis at the detection level. The core location can be easily determined for shower axis falling inside the array; for this reason only "internal events", i.e. events with the core located inside the array, will be firstly analyzed. It should be noted that we need to measure the shower size N_e and not the corresponding primary energy, as the amount of Cherenkov light produced is proportional to the total number of particles in the shower.
The arrival direction of the shower is obtained from the arrival time using the "Time of flight" technique. The arrival direction (for a 2-dimensional simplified scheme) is given by:

$$\text{sen } \alpha = c\, \Delta t / r \tag{5.8}$$

For r = 20 m (separation between 2 detectors), a relative arrival time precision among different detectors $\Delta t \sim 10$ ns is required to obtain an angular resolution of ~ 8.6°. For quasi-vertical showers the position resolution is less relevant in the determination of the arrival direction. For an arrival direction of 20° the same position resolution quoted for the arrival time (3 m) gives a resolution of 3.1° in the arrival direction.

In a scintillator array detector, the particle density measurement is, in first approximation, independent from the arrival direction resolution. In fact, the number of m.i.p. is obtained from the total amount of light collected by the photomultipliers. This light is produced in the detector proportionally to the track length. If *z* is the zenith angle of the impinging particles (equal for all particles), *N* is the total track length of the particles in the scintillator, *S* is the detector surface and ρ is the particle density, the total number of minimum ionizing particles normalized to the vertical direction ($n_{m.i.p.}$) and the detector surface seen by inclined particles (s) are given by:

$$n_{m.i.p.} = N \cos z \qquad s = S \cos z \tag{5.9}$$

$$\rho = n_{m.i.p.}/s = (N \cos z)/(S \cos z) = N/S \tag{5.10}$$

5.2.1 Shower size reconstruction resolution

As discussed, in ULTRA the shower size will be determined and used to reconstruct the yield of incoming Cherenkov light. Thus, an estimation of the resolution on the measurement of this parameter is of crucial importance for the experiment.
The shower size reconstruction resolution depends mainly on the experimental errors and fluctuations of the density measured in each detector. This is strongly dependent on the type and characteristics of the detector. For the proposed detector we have:

a. the Poisson fluctuations on the number of particles crossing the detector;
b. the fluctuations on the energy losses for individual particles;
c. the stability of the photomultipliers gain in time;
d. the fluctuations in light collection, ADC linearity and photocatode non-uniformity.

These effects can be partially calculated (a) and partially measured; the knowledge of the fluctuations on the number of particles (N_p) measured by a detector as a function of N_p is then used to determine the accuracy in the shower size reconstruction analyzing simulated showers.
For each shower the number of particles in each detector is calculated using the NKG formula and fluctuated taking into account all the experimental errors quoted above. The result is then

converted to particle density and used to reconstruct the shower size as for experimental data; the comparison between the input and the reconstructed shower sizes gives the resolution as a function of the shower size.
An example of this technique is shown in figure 19 for the EAS-TOP experiment[8]; a shower size resolution $\sigma_{Ne}/N_e \approx 0.1$ for shower size $N_e > 2 \cdot 10^5$ is quoted.
Since both the ETscope detectors and the array setup are very close to those of the EAS-TOP experiment (in particular: plastic scintillators type and thickness, PMT type, distance between scintillator and photocatode, ADC type) their results can be extrapolated to evaluate the ETscope shower size reconstruction resolution for two detector separations: 20 m and 50 m.
Figure 19 is obtained for a detector surface of 10 m^2 and a detector separation of ~ 70 m; since the fluctuation in the number of particles detected by a single module is a function of the number of particles itself, we can normalize the results to the same number of particles.
From the NKG formula and for a shower size $N_e = 2 \cdot 10^5$ a number of particles $N_p = 20.45$ is expected for a detector of area A = 10 m^2 at a distance d = 70 m.
The same number of particles for a detector of area A = 0.64 m^2 is expected for a shower size $N_e = 3.6 \cdot 10^5$ at d = 20 m and $N_e = 1.6 \cdot 10^6$ at d = 50 m.
The shower size reconstruction resolution is very sensitive to the core location resolution; due to the similar geometry, the same number of particles in each detector and the lower distance among the detectors, the shower core resolution in ETscope is expected to be similar or better (5 m) with respect to EAS-TOP.
The lateral distribution fit (whose integral gives the shower size N_e) is then obtained using 7 points (i.e. detectors) for ETscope and 26 points for EAS-TOP. As a very first approximation we can suppose that the error on N_e is inversely-proportional to the square root of the number of points used in the fit, giving a scale factor $\sqrt{26}/\sqrt{7} = 1.93 \sim 2$.
From these considerations, the expected shower size reconstruction resolution for the ETscope array is:

$$\sigma_{Ne}/N_e = 0.2 \qquad \text{for: } N_e > 3.6 \cdot 10^5 \ (d = 20 \text{ m}) \quad \text{or : } N_e > 1.6 \cdot 10^6 \ (d = 50 \text{ m}) \tag{5.11}$$

corresponding to primary energies of $E = 6.9 \cdot 10^5$ GeV (vertical showers at 2000 m a.s.l.) and $E = 1.9 \cdot 10^6$ GeV (vertical showers at sea level) in the former case (d=20m) and $E = 2.5 \cdot 10^6$

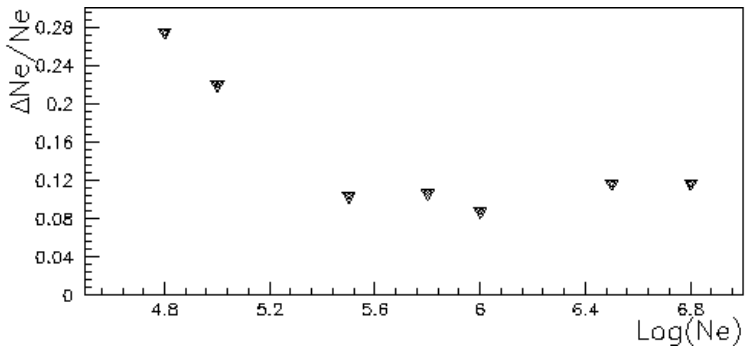

Fig. 19: Shower size reconstruction resolution vs. shower size quoted by the EAS-TOP experiment[8].

GeV (vertical showers at 2000 m a.s.l.) and $E = 6.0 \cdot 10^6$ GeV (vertical showers at sea level) in the case of larger pitch (d=50m).
From figure 19 we can see that for shower sizes (and energies) 3 times lower the corresponding expected shower size reconstruction resolution is ~ 50%.

5.2.2 Energy threshold and counting rate

The main features of an EAS array are the energy threshold and the counting rate. Both of them can be easily obtained from the effective area $A_{eff}(E)$, i.e. the detector surface sensitive to a specific primary energy.
The effective area $A_{eff}(E)$ depends not only on the primary energy but also on the primary particle type (γ,p,Fe,...) and arrival direction. Indeed we will have a set of $A_{eff}(E)$ curves, for each relevant primary particle and slant depth.
The effective area is usually obtained using Monte Carlo (MC) simulations:

1) Showers are developed in the atmosphere using a hadronic interaction model (if needed) up to the observation level and sampling the core location over a trial area centered on the EAS array;
2) The number of particles in each detector is obtained from the lateral distribution of the EAS;
3) The counting fluctuations are taken into account using a Poisson distribution or an experimental one;
4) The triggering conditions are used to verify whether the array has been triggered or not.

This procedure must be repeated for sets of showers with different primary energy, primary particle and zenith angle. For each set, the effective area is given by the projected trial area perpendicular to the shower trajectory multiplied by the number of showers that triggered the array. The trial area must be large enough to include the core of all primaries that could trigger the array.
Performing a complete simulation (i.e. a simulation where all particles including γ,e± are followed) in the energy range we are interested in will require a very large amount of CPU time and disk space. An analytic approach can be used to simplify this job, using a parameterization of the electromagnetic branches of the hadronic cascade or using analytic approximations like (2.1) and (2.5) for the longitudinal and lateral distributions. However, using this strategy it is difficult to take into account the fluctuations, leading to a bad estimation of the detector performance mainly near the threshold energy of the array.
Once the $A_{eff}(E)$ function is determined, the threshold energy is usually defined as the mode of the distribution:

$$n(E)dE = A_{eff}(E)\, \Phi(E)\, dE \tag{5.12}$$

where:

$$\Phi(E)\, dE = I_0\, E^{-\gamma}\, dE \tag{5.13}$$

is the primary flux of cosmic ray particles and the mode of a distribution $y = f(x)$ is the value of x for which the y reaches its maximum value.
The counting rate for primaries with $E>E_0$ will be:

$$N = I_0 \Delta T \Delta \Omega \int_{E_0}^{\infty} E^{-\gamma} A_{eff}(E) dE \qquad (5.14)$$

where $\Delta\Omega$ is the solid angle and ΔT is the integration time.
For this array a semi-empirical method, based on the extrapolation of experimental results measured by a similar array, has been used.
The EAS-TOP array[18] was located at 2005 m a.s.l., corresponding to 810 g cm^{-2}; 4 detectors, 10 m^2 of plastic scintillator each, where located at the corners of a square 17 m side.
The quoted rate for the 4-fold coincidence was 5.3 Hz and the threshold energy E_{th} = 30 TeV.
Using the cosmic ray all particle spectrum shown in figure 20 (from a collection of experimental data done by S.Swordy) we obtain:

$$\Phi(E>30TeV) = 4.13 \cdot 10^{-4}\ m^{-2}\ s^{-1}\ sr^{-1} \qquad (5.15)$$

$$A_{eff} = 5.3/(4.13 \cdot 10^{-4}\ \pi)\ m^2 \sim 4000\ m^2 \qquad (5.16)$$

($\Delta\Omega = \pi$ sr corresponds to an opening angle of 60º for isotropic (spheric) detectors and 90º for horizontal (flat) detectors).
We can see that the effective area is ~ 10 times greater than the enclosed area. Using the longitudinal distribution (2.1) for the quoted atmospheric depth and the lateral distribution (2.5) at 24 m (corresponding to the square diagonal) we obtain for the shower size and for the number of particles in a detector module, respectively:

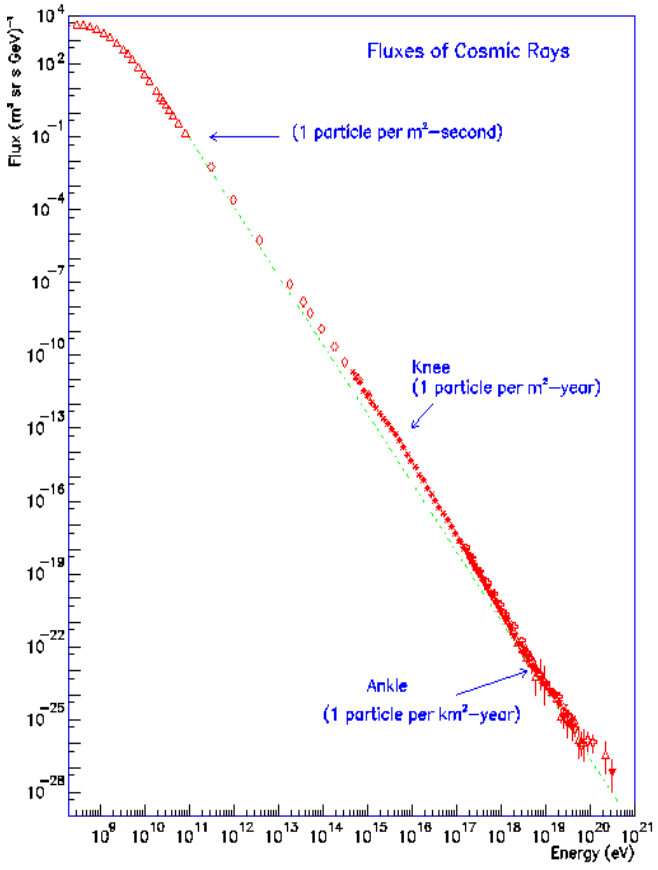

Fig. 20: All particles differential energy spectrum of cosmic rays.

$$N_e(E = 30\ \text{TeV}, t = 810\ \text{gcm}^{-2}) = 7.0 \cdot 10^3\ \text{(vertical showers)} \qquad (5.17)$$

and

$$N_p(r=24\ \text{m}, S=10\ \text{m}^2) = 4.8 \qquad (5.18)$$

For the ETscope array, at sea level, with a detector surface S=0.64 m^2 and a distance between adjacent detectors of 20 m we have the same number of particles for $N_e = 8.5 \cdot 10^4$ (N_p(r=20 m,S=0.64 m^2)=4.8).
For vertical showers this corresponds to a primary energy of $6.4 \cdot 10^{14}$eV (N_e=$8.6 \cdot 10^4$) at sea level and $2.1 \cdot 10^{14}$eV (N_e=$8.6 \cdot 10^4$) at 2000 m a.s.l..
Using these values as threshold energy, a solid angle of π sr and an area of $\pi r^2 = \pi \cdot 20^2 = 1.3 \cdot 10^3$ m^2 we can estimate the expected rate of internal events:

$$\Phi(E > 6.4 \cdot 10^{14}\ \text{eV}) = 2.9 \cdot 10^{-6}\ \text{m}^{-2}\ \text{s}^{-1}\ \text{sr}^{-1} \qquad (5.19)$$

$$n_{int}(E > 6.4 \cdot 10^{14}\ \text{eV}) = \Phi(E > 6.4 \cdot 10^{14}\ \text{eV})\ \Delta\Omega A_{int} = 0.012\ \text{Hz} = 41\ \text{events/h} \qquad (5.20)$$

$$\Phi(E > 2.1 \cdot 10^{14}\ \text{eV}) = 1.8 \cdot 10^{-5}\ \text{m}^{-2}\ \text{s}^{-1}\ \text{sr}^{-1} \qquad (5.21)$$

$$n_{int}(E > 2.1 \cdot 10^{14}\ \text{eV}) = \Phi(E > 2.1 \cdot 10^{14}\ \text{eV})\ \Delta\Omega A_{int} = 0.070\ \text{Hz} = 252\ \text{events/h} \qquad (5.22)$$

The expected trigger rate for all events, including external events, is 10 times higher.
Table 1 summarizes the performances of the ETscope array for 2 detector separations (20m and 50m) and 2 atmospheric depth locations (sea level and 2000 m a.s.l.). We can see that all the energy region between $2 \cdot 10^{14}$ eV and $2 \cdot 10^{15}$ eV can be explored with reasonable rates of internal events, from which all the relevant shower parameters can be accurately measured.
The results obtained with this method are very straightforward, giving a first estimation of the threshold energy and counting rates without any MC program development; anyway the estimations could be very rough and an accurate evaluation of the effective area for both internal and external events based on the procedure described at the beginning of this section is strongly needed.

Table 1: Expected threshold energy and internal event counting rate of the ETscope array for two different detector separations and two different observation levels.

Array radius (m)	Atm. depth (g cm^{-2})	Thres. Energy (E_{th}, GeV)	$\Phi(E>E_{th})$ (m^{-2} s^{-1} sr^{-1})	$n_{int}(E>E_{th})$ Hz	ev./h
20	810	$2.1 \cdot 10^5$	$1.8 \cdot 10^{-5}$	0.070	252
20	1013	$6.4 \cdot 10^5$	$2.9 \cdot 10^{-6}$	0.012	41
50	810	$7.0 \cdot 10^5$	$2.5 \cdot 10^{-6}$	0.062	224
50	1013	$1.9 \cdot 10^6$	$4.9 \cdot 10^{-7}$	0.012	44

5.3 Laser measurements

Laser measurements are essential for the determination of the atmospheric transmission along the path from the ETscope array to the UVscope. Cherenkov signal reflectively diffused

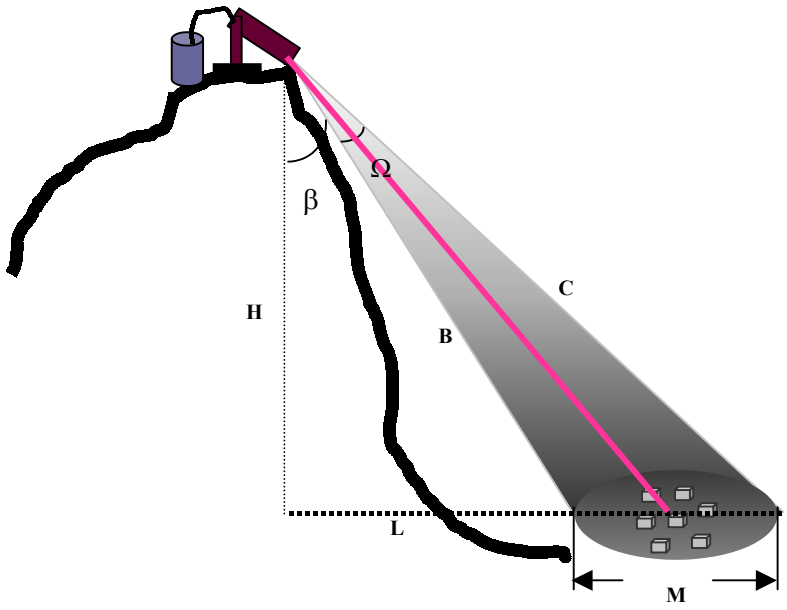

Fig. 21: Sketch of the Laser configuration in ULTRA.

by target-surfaces undergoes attenuation due to the scattering of light in the atmosphere. This attenuation is variable in time and depends on the local environmental conditions. The major

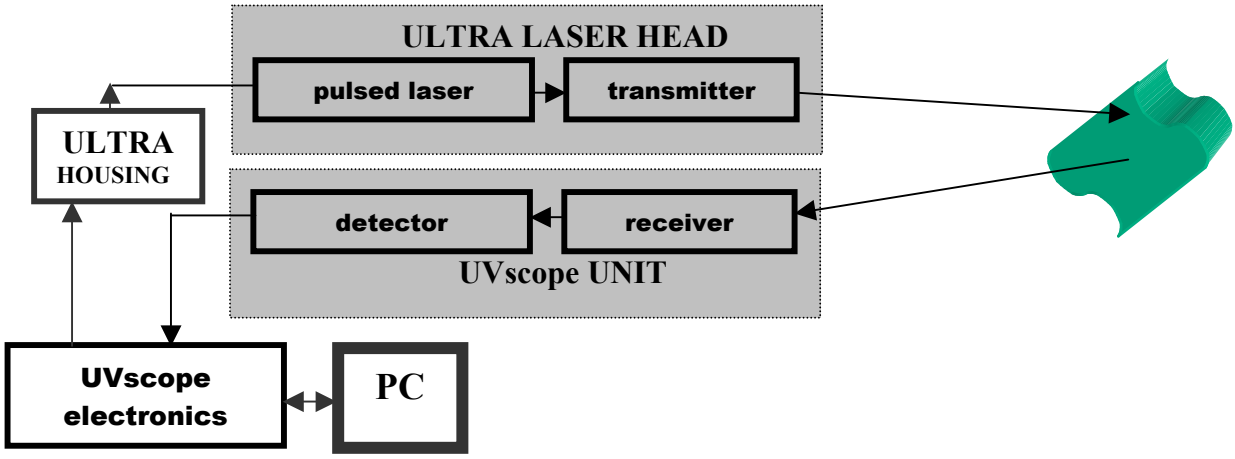

Fig. 22: Schematic block diagram of the Laser system. In the shown configuration the Laser unit is the transmitter and an UVscope unit the receiver.

contributions to light attenuation is due to molecular scattering and aerosol scattering. The main purpose of the Laser is the measurement in situ of the global atmospheric transmission, without the need of separating the different contributions. During each acquisition run, timed Laser shooting permits to measure periodically the atmospheric attenuation factor.

Figure 21 shows the Laser arrangement as foreseen for the ULTRA experiment. A brief description of the parts (subsystems) constituting the overall Laser system is schematically

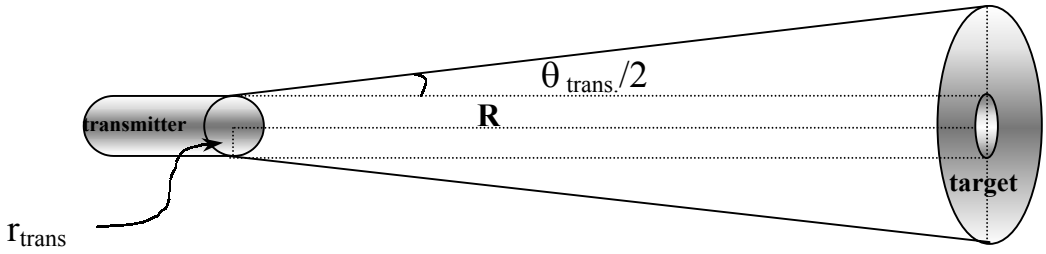

Fig. 23: Transmitter-target geometry.

represented in figure 22. The transmitter and the receiver modules shown in the figure are both optical systems. The transmitting optical system reduces the divergence angle of the transmitted beam and directs the light beam to the target. The receiver optical system collects part of the reflected light beam and focuses it into the detector. The Uvscope electronics triggers the Laser pulse and measures the light intensity received back at the detector. The photon events are stored individually in a PC memory.

Once the number of photoelectrons N_{pe} has been measured by an UVscope unit to find the reflectivity coefficient, equation (5.3) must be solved for R. However, two unknown quantities still remain, P_c and $T(\lambda)$. While P_c is given by the measurement of the shower size with ETscope, $T(\lambda)$ must be measured independently. This can be done using Laser beam and receiver optics as proposed here. To establish the required transmission energy, detector sensitivity and optical aperture it is indispensable to discuss the geometrical factors that affect the relation between transmitted energy and received energy. In the following discussion it is assumed that the transmitted beam completely covers the entire area of the target that reflects the beam back to the source. The transmitter to target geometry of the Laser light beam is shown in figure 23. At the target plane, a distance R from the transmitter, the lit area from the transmitter is:

$$A_{target} = \pi \cdot (r_{trans} + \theta_{trans.}/2)^2 \qquad (5.23)$$

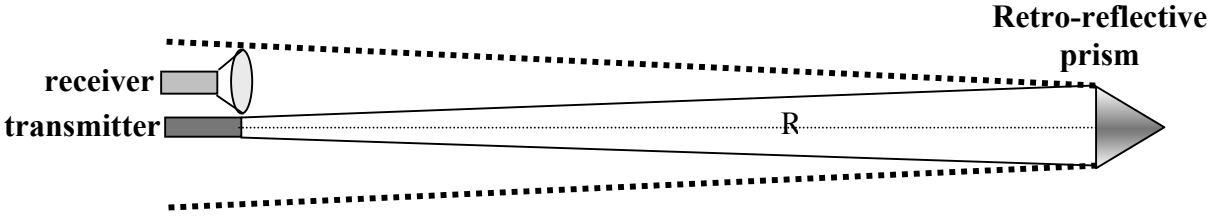

Fig. 24:Transmitter-Receiver to retro-reflective prism geometry.

The energy density Φ_{target} within this area is equal to the transmitter energy $\mathbf{E_{trans}}$ divided by the lit area $\mathbf{A_{target}}$ and reduced by the atmosphere transmission T:

$$\Phi_{target} = E_{trans} \cdot T(\lambda) / A_{target} \qquad (5.24)$$

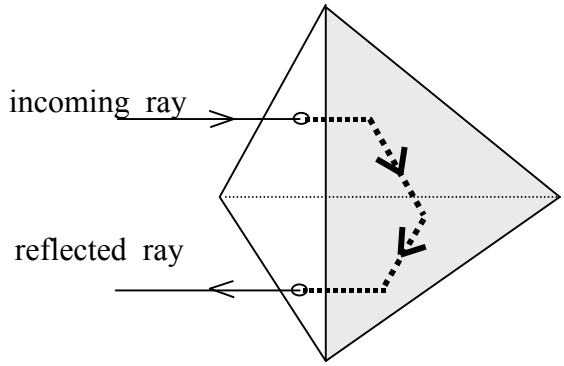

Fig. 25: Total internal reflection of a ray from a retro-reflective cube corner.

The value of **T(λ)** varies from 0 to 1, depending on the amount of absorption and scattering of light by the atmospheric condition. As mentioned above, **T(λ)** has to be measured and this is accomplished by placing a retro-reflective device on the target as shown in figure 24. A common retro-reflector device is the "cube corner reflector". This device is an optical prism with three plane faces orthogonal to each other. The characteristics of this prism are such that a light ray entering the non-orthogonal face undergoes total internal reflection at each of the other three faces as shown in figure 25. After reflection from each of the three faces, the light ray raise from the same face that it entered. The exit beam is parallel to the entrance beam so that the beam appears to have been reflected by a plane mirror whose surface is perpendicular to the beam axis. This type of reflector gives a return beam independent of the exact orientation of the prism, so that alignment is not critical. The emerging beam has a divergence angle equal to the divergence of the intercepted rays from the transmitter plus diffraction effects due to the limited size of its aperture. Assuming a reflectivity for the corner reflector of 100%, the returned energy in the case of a retro-reflector cube is:

$$E_{\text{target reflected}} = \Phi_{\text{target}} \cdot A_{cc} \tag{5.25}$$

where A_{cc} is the effective area of the corner cube reflector. The divergence angle θ_{cc} (in radians) of the return beam from the retro-reflector is given by:

$$\theta_{cc} = d_{cc}/R + 2.44\,\lambda/\,d_{cc} \tag{5.26}$$

where $\mathbf{d_{cc}}$ is the diameter of the corner cube, λ is the wavelength of the laser transmitter and R is the distance from the transmitter to the corner cube reflector. From the divergence angle, the area of the return beam at the receiver can be calculated using the (5.23) as follows:

$$A_{\text{return}} = \pi/4 \cdot (\theta_{cc} \cdot R + d_{cc})^2 = \pi/4 \cdot (d_{cc} + 2.44\,\lambda \cdot R/\,d_{cc} + d_{cc})^2 \tag{5.27}$$

The energy density of the return beam at the receiver is:

$$\Phi_{\text{return}} = E_{\text{target reflected}} \cdot T(\lambda)/A_{\text{return}} \tag{5.28}$$

and the energy received by the optical receiver E_{rec} is:

$$E_{rec} = \Phi_{return} \cdot A_{rec} \qquad (5.29)$$

Combining equations (5.24) to (5.29) gives:

$$E_{rec} = E_{trans} \cdot d^2_{cc} \cdot d^2_{rec} \cdot T^2(\lambda) / [(\theta_{trans} \cdot R + d_{trans})^2 \cdot (2\, d_{cc} + 2.44\, \lambda \cdot R / d_{cc})^2] \qquad (5.30)$$

where the d_{rec} is the diameter of the receiver optical system and d_{trans} is the diameter of the transmitter optical system. Finally the total number of photoelectrons collected by the receiver is:

$$N_{perec} = \lambda \cdot E_{rec} \cdot \varepsilon_{tot} / 1240 \qquad (5.31)$$

with λ the laser wavelength in nm and ε_{tot} the total collecting efficiency of the receiver optical system.
Laser can be used in ULTRA for other applications. For example using a transmitting diffuser to enlarge the divergence angle of the laser beam should be possible to measure the reflectively/diffused signal from test surfaces of known reflection coefficient placed like a floor layer at the ETscope site. Such type of material is the PVC "Marvic"and a high-density polyethylene (HDPE) Tyvek[19].

6. CONCLUSIONS AND SCHEDULE

The ULTRA experiment has been proposed in the framework of the EUSO experiment as a test to evaluate the possibility of detecting the Cherenkov signal from space. Nevertheless this measurement makes sense by itself, due to the general lack of data in this field (all the experiments have measured up to now the Cherenkov light reflected only by snow and with no informations about the associated EAS).
Moreover the ULTRA experiment objectives cover a parallel subject, since the same detector (UVscope) at the same location, sharing people and logistics, can be used for meteors measurement, giving valuable informations in a field poorly covered by present experiments.
In addition the UVscope detector, carried on balloon flights, will continue the atmospheric background measurements done up to now with BABY.
We have thus a multi-purpose experiment, dedicated to EUSO but able to make physics by itself.

The first evaluations presented in this report show that the ULTRA detector can accurately measure with full efficiency and reconstruct the relevant parameters of EASs with $E > 10^{16}$ eV. Few events per hour are expected in this energy range; but we think that ~100 events well characterized for every experimental setup, i.e. for different reflecting/diffusing surfaces and shower axis inclinations, are enough for our purposes.
All the evaluations reported here are analytical or obtained extrapolating the results from other experiments; a MonteCarlo simulation specific for our experiment for both Cherenkov and electro-magnetic components is certainly needed. The detectors response measured on-site and the laser measurements will give the necessary inputs for the experiment simulation.

The first measurement campaign has been performed during October 2002 at Mont-Cenis with an array of 4 detectors and the BABY telescope for the UV light measurement[20].
During this campaign we have:

1) Checked and solved the logistic problems;
2) Checked data acquisition;
3) Calibrated the ETscope detector;
4) Measured the trigger rate as a function of detectors separation;
5) Started laser tests.

Next measurements are scheduled for the end of June 2003 at the same location with an improved ETscope (5 detectors) and the first UVscope unit.
During this campaign the detection of correlated events (ETscope + UV detector), that was not possible with BABY due to the very narrow field of view, is of crucial importance for our experiment.
These first measurements have been done with the ETscope array on ground; a test in water is foreseen immediatly after next campaign.
The following development will be linked to the general EUSO schedule and to the first test results.

7. REFERENCES

(1) L.Scarsi et al., "EUSO – Extreme Universe Space Observatory", Proposal for the ESA F2/F3 Mission, http://www.ifcai.pa.cnr.it/EUSO/docs/EUSOproposal.pdf and references therein, (2000).
(2) R.Andresen et al.,"Extreme Universe Space Observatory – EUSO. Report on the accommodation of EUSO on the Columbus Exposed Payload Facility". ESA/MSM-GU/200.462/AP/RDA, (2000).
(3) O.Catalano et al., Nucl. Instrum. Meth. A, **480/2-3**, 547, (2002)
(4) B.Biondo et al., "Air Fluorescence Efficiency Measuements for AirWatch based mission: Experimental Set-up", in "Observing giant cosmic ray air showers", J.F. Krizmanic, J.F.Ormes, R.E.Streitmatter (Eds), AIP Conference Proceedings No.**433**, 361, (1998).
(5) K.Greisen, Progr. in Cosmic Ray Physics, **3**, 1, (1956).
(6) K.Kamata et al., Prog. Theor. Phys. Suppl. **6**, 93, (1958).
(7) O.Catalano, G.D'Alì Staiti, M.Gabriele and L.La Fata, Proc. ICRC 2001, 498, (2001).
(8) M.Aglietta et al., Nucl. Instrum. Meth. A, **336**, 310, (1993).
(9) A.E.Chudakov, Proc. Symp On Cosmic Rays, Yakutsk, 69, (1972).
(10) C.Castagnoli, G.Navarra, C.Morello, Il Nuovo Cimento 6C, **2**, 202, (1983).
(11) R.A.Antonov, D.V.Chernov, A.N.Fedorov, E.A.Petrova, Nuclear Physics (Proc. Suppl.) **52B**, 182, (1997).
(12) I.Angelov, I.Kirov, E.Malamova, J.Stamenov, Proc. ICRC 2001, 900, (2001).
(13) H.C.Van de Hulst, "Light scattering by small particles", J.Wiley and Sons, New York, (1957).
(14) R.M.Baltrusaitis et al., Nucl. Instrum. Meth. A, **240**, 410, (1885)
(15) L.Rayleigh, "The theory of sound", 3rd ed. MacMillan, London, (1896).
(16) Philips, Photomultipliers Data Handbook, Book PC04, 389, (1990).
(17) P.Assis, Presentation at the EUSO IWG meeting, Faro, (2002).
(18) M.Aglietta et al., Nucl. Instrum. and Meth. A, **277**, 23, (1989).
(19) Auger project, Design report, (1996).
(20) J.Chauvin et al., "The ETscope Ground Array for the ULTRA Experiment", Proc. ICRC 2003, in press.